THE ASTROPHYSICAL JOURNAL, 449:527–549, 1995 August 20

LARGE-SCALE STRUCTURES IN THE ZONE OF AVOIDANCE: THE GALACTIC ANTICENTER REGION

NANYAO Y. LU
Jet Propulsion Laboratory, MS 100-22, California Institute of Technology, Pasadena, CA 91125; lu@ipac.caltech.edu
AND
WOLFRAM FREUDLING
Space Telescope—European Coordinating Facility, European Southern Observatory, Karl-Schwarzschild-Strasse 2, 85748 Garching bei München, Germany; wfreudli@eso.org
Received 1994 June 2; accepted 1995 March 1

ABSTRACT

We have selected a sample of 876 galaxy candidates from the *IRAS* Point Source Catalog in the region of $2^h < \alpha < 10^h$ and $0° < \delta < 36°$, which crosses the Galactic anticenter part of the Zone of Avoidance (ZOA) and includes most of the highly obscured Orion-Taurus complex region. We have identified galaxies among the candidate sources by attempting to detect the 21 cm H I line of those sources which were not known to be galaxies at the beginning of the survey. In this manner, we constructed a galaxy sample which is largely free from Galactic reddening.

Of the 272 observed candidates, 89 were detected in the H I line up to a heliocentric velocity of $v_h \approx 16{,}000$ km s^{-1}. The resulting galaxy sample of 717 galaxies is fairly complete (within about 10%) and uniform (within about 4%) in the part of the survey area 10° away from the Galactic plane and for velocities up to at least 9000 km s^{-1}. This provides, for the first time, a largely unbiased view on the large-scale structures in much of the survey area. Our main results are the following: (1) Several large voids are identified. In particular, a void between $\alpha \approx 3^h$ and 4^h, up to $v_h \sim 6000$ km s^{-1}, separates the Pisces-Perseus supercluster at $\alpha < 3^h$ from structures at $\alpha > 4^h$; and a "nearby void" occupies most of our survey area and reaches out to a redshift of nearly 3000 km s^{-1}. (2) We found no nearby galaxy concentration that could significantly contribute to the "Local Velocity Anomaly" (LVA), but a general excess of galaxies around $v_h \sim 5000$ km s^{-1} in the survey area. (3) The contrast between the "Great Wall" at $v_h \sim 8500$ km s^{-1} and the void in front of it appears to gradually diffuse out after it enters the Zone of Avoidance from the northern Galactic hemisphere. (4) Our data combined with other galaxy surveys in or near the Galactic anticenter part of the ZOA suggest that the main ridge of the Pisces-Perseus supercluster does also not extend to Abell 569, a cluster in the northern Galactic hemisphere, and that the simple gravitational model consisting of the Local Void of Tully & Fisher, our nearby void, and Puppis and Fornax-Eridanus clusters would predict a LVA whose direction is probably too far away from that derived from observations.

Subject headings: galaxies: clustering — galaxies: distances and redshifts — radio lines: galaxies

1. INTRODUCTION

Galaxies have been identified optically in the Zone of Avoidance (ZOA) with or without using *IRAS* positions (e.g., Böhm-Vitense 1956; Fitzgerald 1974; Dodd & Brand 1976; Weinberger 1980; Saitō et al. 1990, 1991; Kraan-Korteweg 1991; Yamada et al. 1993; Takata et al. 1994; Kraan-Korteweg & Woudt 1994; Seeberger et al. 1994b; Wakamatsu 1994). While optically generated galaxy samples are quite uniform at high Galactic latitudes, they become highly nonuniform near the Galactic plane ($|b| \lesssim 30°$) and in regions of excessive and patchy reddening, making it difficult and often ambiguous to interpret the observed galaxy distribution in the ZOA. Blind 21 cm H I surveys can produce uniform samples (e.g., Kerr & Henning 1987; Kraan-Korteweg et al. 1994; Henning 1994), but are very time consuming to be carried out over large regions in the sky.

By contrast, the *IRAS* Point Source Catalog (Version 2, 1988, hereafter PSC) is fairly uniform above a few degrees in Galactic latitude and away from the Galactic center, and contains primarily gas-rich spiral galaxies. This fact has been exploited to select galaxy candidates from the PSC, and identify galaxies among them by follow-up 21 cm H I observations (e.g., Lu et al. 1990). The selection of such a galaxy sample is almost independent of galactic extinction, and therefore offers a largely unbiased view of the large-scale structure in and across the ZOA. The results of such an approach can also be easily integrated into existing *IRAS* redshift surveys outside the ZOA (e.g., Strauss et al. 1990; Rowan-Robinson et al. 1991; Fisher et al. 1992) to compare the large-scale structure in the ZOA with the one in other regions of the sky.

In this paper, we applied this "extinction-free" approach to the region $2^h < \alpha < 10^h$ and $0° < \delta < 36°$. This region is approximately opposite to the Galactic center, and is referred to as the "anticenter region" throughout this paper. The part of this region with $b < 10°$, which contains most of the highly obscured Orion-Taurus region, is of interest for several reasons: (1) The region was always left out of previous redshift surveys because of its high and patchy Galactic extinction. (2) The observed "Local Velocity Anomaly" of the Local Group is pointing towards this region (Faber & Burstein 1988; Han & Mould 1990), suggesting that a nearby galaxy concentration (i.e., cluster or supercluster) which generates such motion might be hidden in this region. (3) The galaxy excess associated with the Pisces-Perseus (hereafter PP) supercluster can be

visually traced within this declination range up to $\alpha \lesssim 3^h$. Despite extensive studies of the PP region (e.g., Haynes & Giovanelli 1988; Giovanelli & Haynes 1993, and references therein; Hauschildt 1987; Chamaraux et al. 1990; Maurogordato, Proust, & Balkowski 1991; Seeberger et al. 1994b), no redshift survey has been specifically undertaken at these low Galactic latitudes. It is therefore not known whether the PP supercluster extends to $\alpha > 3^h$. (4) The suggested large structure nicknamed "Gereat Wall" (Geller & Huchra 1989) stretches from the northern Galactic hemisphere all the way to the ZOA. A better determination of the characteristic length of this largest known coherent structure can put a tighter constraint on large-scale structure formation scenarios. It is therefore particular interesting whether this structure extends to the Orion-Taurus region.

The remainder of this paper is organized as follows: We present the sample selection, 21 cm radio observations and results in § 2. In § 3 we construct our galaxy sample by combining the newly identified galaxies with previously known ones, and discuss its completeness and uniformity. We describe the angular and redshift distributions of our galaxy sample in § 4. In § 5 we consider the galaxy distribution over a larger area in the general Galactic anticenter part of the ZOA, and discuss the extent of the PP supercluster and the origin of the Local Velocity Anomaly. Finally we summarize our results in § 6.

2. THE 21 CENTIMETER H I SURVEY

2.1. *Sample Selection*

Spiral galaxies in the local universe were readily detected by *IRAS*. Therefore, galaxy samples drawn from the PSC are thought to be a uniform and fair sample of the large-scale structure (Strauss et al. 1990). Because Galactic extinction in *IRAS* bands is negligible, this is true even for low Galactic latitudes except for areas where the PSC itself may become highly nonuniform (see § 3). However, in heavily obscured regions, the number of Galactic sources in the PSC is also high. Therefore, in order to obtain a reasonably sized sample of galaxy candidates, one needs to preselect galaxy candidates from the PSC sources according to criteria which discriminate against Galactic sources. We used the selection criteria given in Lu et al. (1990), which have been shown to be very efficient in screening out Galactic sources, while still including more than 50% of the *IRAS* galaxies down to a few degrees in Galaxies latitude (Lu et al. 1990; Meurs 1994). The selection criteria, which are discussed in detail in Lu et al. (1990), are listed in Table 1 and briefly summarized here. The flux criterion, $1.5 < f(100) < 8$ Jy, where $f(100)$ is the *IRAS* flux density at 100 μm (and similar notations for the other *IRAS* bands), is preferred over $f(60)$ for our H I observations because of its tighter correlation with the 21 cm line flux. The employed upper limit is necessary for low Galactic latitudes where there are large numbers of bright Galactic sources. The drawback is the exclusion of some nearby bright galaxies: at a distance of 1000 km s^{-1}, the ratio of the number of PSC galaxies with $f(100) > 8$ Jy to that with $1.5 < f(100) < 8$ Jy is roughly unity; while at 3000 km s^{-1}, this ratio becomes about 0.15. The next two color criteria in Table 1 exclude most of the stars. The far-infrared (FIR) color criterion in terms of $f(60)/f(100)$ matches the colors of most IR-normal galaxies, while its upper limit excludes warm Galactic sources (e.g., H II regions) and its lower limit excludes cold Galactic cirrus sources. Most galaxies in the current *IRAS* flux range of interest are point sources with respect to the *IRAS* beam, we therefore selected only those sources with a PSC point-source correlation coefficient (which measures the degree of the spatial extension of a source; see *IRAS* Explanatory Supplement 1988) larger than or equal to 0.98 at both 60 and 100 μm. This criterion is particularly efficient at filtering out Galactic sources which are usually more extended than galaxies. Finally, we only select sources whose 100 μm flux densities have a moderate to good quality. Applying our criteria to optically cataloged galaxies in the PSC at high Galactic latitudes ($|b| > 35°$) indeed selects at least 50% of all galaxies at all redshifts. The selection criteria have an effective cutoff at about 0.65 Jy in the flux density at 60 μm, a value that is useful in comparing our sample with some existing *IRAS* galaxy samples selected at 60 μm (e.g., Strauss et al. 1990; Rowan-Robinson et al. 1991).

TABLE 1

INFRARED SELECTION CRITERIA

Parameter	Criteria
PSC flux density at 100 μm	$1.5 < f(100) < 8$ Jy
PSC flux quality at 100 μm	moderate or high
PSC flux density ratios	$f(25)/f(100) < 0.50$
	$f(12)/f(100) < 0.17$
	$1.13 < f(100)/f(60) < 4.00$
PSC correlation coefficients (CC).....	$CC(60) \geq 0.98$; $CC(100) \geq 0.98$

NOTE.—$f(x)$ is the PSC flux density at x μm, with $x = 12, 25, 60$, or 100.

A total of 876 sources were selected from the PSC using these criteria. Their *IRAS* names and Galactic latitudes in degrees are listed in columns (1) and (2) of Table 2. The sample contains sources of three different categories: (1) 462 (53%) "cataloged galaxies," i.e., sources flagged in the PSC to be associated with one or more optical galaxy catalogs; (2) 47 (5%) "Galactic sources" (as marked in the PSC); and (3) 367 (42%) pure *IRAS* sources. The numeric index (of 1 to 3) in column (3) of Table 2 indicates to which category a source belongs. A nonzero number in column (4) indicates that the sample source was observed in one of two similar 21 cm H I surveys over a velocity coverage of (0–8000) km s^{-1}, where 1 = the current survey and 2 = Lu et al. (1990). Similarly, an index of unity in column (5) means that the source was observed in the current survey over a velocity coverage of (8000–16,000) km s^{-1}. If a heliocentric velocity, v_h, is available for an identified galaxy, it is given in column (6) in units of km s^{-1}. For galaxies we list in column (7) a reference that gives either the original redshift or identification, or the original work of the redshift or identification. The reference codes are: 1 = this paper, 2 = Lu et al. (1990), 3 = Pantoja et al. (1994), 4 = Giovanelli & Haynes (1993), 5 = the third Reference Catalogue of Galaxies (de Vaucouleurs et al. 1993), 6 = the NASA/IPAC Extragalactic Database (hereafter NED; Helou et al. 1991), 7 = Strauss et al. (1992), 8 = the "*IRAS*-1.2Jy" redshift catalog (Strauss 1994; also see Fisher et al. 1992), 9 = the "1-in-6" redshift catalog of the Queen Mary-West Field College, Durham, Oxford, and Toronto (hereafter QDOT; Lawrence et al. 1994), 10 = Takata et al. (1994), and 11 = the catalog of *IRAS* point source redshift survey (hereafter PSC-Z; Saunders 1994; also see Rowan-Robinson et al. 1991). Also included in Table 2 are an additional sample of 23 PSC sources (marked by an asterisk following their names) which fail to pass our selection criteria. H I observations of these sources are used in

TABLE 2

LIST OF THE CANDIDATE SOURCES

Name (1)	b (2)	n1 (3)	n2 (4)	n3 (5)	v_h (6)	ref (7)	Name (1)	b (2)	n1 (3)	n2 (4)	n3 (5)	v_h (6)	ref (7)	Name (1)	b (2)	n1 (3)	n2 (4)	n3 (5)	v_h (6)	ref (7)
02011+1925	-40	1	0	0	8491	6	02213+2541	-32	3	1	1	-	-	02406+1627	-39	1	0	0	7641	6
02014+2824	-32	1	0	0	4591	6	02218+2518	-33	1	0	0	10470	6	02407+0445	-48	1	0	0	4088	5
02015+0232	-55	1	0	0	6332	6	02221+2549	-32	1	0	0	10080	6	02407+3217	-25	1	0	0	4134	11
02022+2052	-39	3	0	0	8977	7	02224+2402	-34	1	0	0	9711	6	02410+0728	-46	1	0	0	6406	11
02023+3432	-26	1	0	0	4412	6	02226+2010	-37	1	0	0	3900	6	02411+0354	-49	3	1	1	-	8
02025+3056	-29	1	0	0	5276	6	02239+1910	-38	3	1	0	4189	1	02416+1722	-38	1	0	0	7765	4
02025+0941	-49	1	0	0	7766	6	02240+2448	-33	1	0	0	9641	6	02420+0507	-48	1	0	0	-	11
02025+3438	-26	1	0	0	4412	6	02245+2252	-35	1	0	0	9545	11	02427+1843	-36	1	1	0	-	8
02044+3243	-27	1	0	0	11130	6	02246+2526	-32	1	0	0	5085	6	02428+0240	-49	1	0	0	6793	5
02048+1657	-42	1	0	0	4514	6	02248+2621	-32	1	0	0	9786	6	02432+0301	-49	1	0	0	-	11
02050+3457	-25	1	0	0	-	6	02249+2740	-30	3	1	1	10468	1	02433+1544	-39	3	1	1	7876	1
02051+2805	-32	1	0	0	-	6	02252+3105	-27	1	0	0	4993	6	02437+1842	-36	3	1	1	9957	1
02056+2859	-31	1	0	0	6576	6	02256+2156	-35	3	1	1	9043	1	02438+0323	-49	1	0	0	6789	5
02057+1406	-45	1	0	0	4422	6	02264+3125	-27	1	0	0	5231	6	02438+2122	-34	3	0	0	6987	6
02057+1444	-44	1	0	0	4405	6	02271+2826	-29	3	1	0	4565	1	02440+2323	-32	1	0	0	6190	5
02062+0744	-50	1	0	0	3458	6	02280+2209	-35	3	0	0	9619	7	02444+1619	-38	3	1	1	8517	1
02063+3314	-27	1	0	0	11580	6	02281+2728	-30	1	0	0	4617	6	02445+1510	-39	1	0	0	7214	11
02073+2336	-36	3	1	1	-	-	02284+2021	-37	3	1	1	-	-	02450+0425	-48	1	0	0	6364	5
02076+3111	-29	3	1	1	14166	1	02288+2241	-34	1	0	0	5870	6	02451+2653	-29	1	0	0	5648	6
02077+2255	-36	3	1	1	14132	1	02290+2533	-32	3	1	0	15557	7	02451+0522	-47	3	1	1	1519	1
02079+0537	-52	1	0	0	4569	6	02293+3516	-23	1	0	0	601	6	02451+0012	-51	1	0	0	-	11
02080+3103	-29	1	0	0	5068	7	02302+3231	-25	1	0	0	5229	6	02461+2618	-29	3	1	1	17387	9
02083+2534	-34	1	0	0	5128	6	02304+2210	-35	1	0	0	5431	6	02463+0257	-49	1	0	0	4172	5
02086+3348	-26	1	0	0	6175	6	02311+1059	-44	1	0	0	7282	11	02465+3349	-23	1	0	0	11550	6
02088+1340	-45	1	0	0	7966	6	02313+3217	-26	1	0	0	4851	5	02467+3446	-22	1	0	0	5138	6
02093+2929	-30	3	1	1	9232	1	02315+2621	-31	3	1	1	10882	1	02468+1803	-36	3	1	1	-	-
02108+1651	-42	1	0	0	11040	6	02315+3439	-23	1	0	0	-	8	02471+1646	-37	3	1	1	11862	1
02111+0352	-53	1	0	0	3436	6	02334+3129	-26	1	0	0	5100	6	02477+2654	-29	3	1	1	-	-
02111+2738	-32	1	0	0	567	6	02335+3454	-23	3	1	0	-	-	02483+0319	-48	1	1	0	-	8
02118+3114	-28	1	0	0	5276	6	02337+3553	-22	1	0	0	5130	5	02487+1548	-38	1	0	0	16469	5
02129+3334	-26	1	0	0	9631	11	02338+3306	-25	1	0	0	4534	6	02491+2113	-33	3	1	1	8517	1
02132+2901	-30	3	1	1	-	-	02338+0029	-52	1	0	0	6584	5	02493+0902	-43	3	1	1	15215	1
02133+2822	-31	1	0	0	2995	6	02342+2738	-29	3	1	1	-	-	02514+0245	-48	1	0	0	3042	5
02144+1419	-43	1	0	0	3736	6	02355+3212	-25	3	1	1	25508	7	02523+0854	-43	3	1	1	-	8
02146+2917	-30	1	0	0	5197	6	02358+0145	-51	1	0	0	5876	9	02530+1004	-42	3	1	1	-	8
02146+1605	-42	3	1	0	4040	1	02358+3424	-23	1	0	0	4782	5	02537+0853	-43	3	1	1	10959	1
02150+2201	-36	1	0	0	13396	7	02359+3523	-22	1	0	0	9243	6	02539+0913	-43	1	1	1	7382	1
02150+3139	-28	1	0	0	6062	6	02362+0853	-45	1	0	0	5125	5	02540+0707	-44	1	0	0	8143	5
02153+2636	-32	3	0	0	15016	7	02370+1748	-38	1	0	0	8552	5	02543+0600	-45	1	0	0	6372	6
02158+0525	-51	1	0	0	9093	6	02370+2807	-29	3	0	0	10950	6	02546+0234	-47	1	0	0	3213	5
02167+2420	-34	3	1	1	-	-	02373+3202	-25	1	0	0	4488	5	02552+2349	-30	1	0	0	10440	6
02172+2947	-29	1	0	0	11771	6	02376+1904	-37	1	0	0	783	6	02552+3208	-23	1	0	0	3610	6
02175+3506	-24	3	0	0	-	8	02382+2758	-29	3	1	1	-	-	02558+0606	-45	1	0	0	6708	5
02178+3228	-27	1	0	0	10020	6	02382+0822	-46	1	0	0	5435	5	02569+1022	-41	3	1	1	7420	1
02183+2254	-35	3	1	1	-	-	02390+3448	-23	3	1	1	-	-	02571+1623	-36	3	1	1	9327	1
02185+0642	-50	3	0	1	-	8	02391+0202	-50	3	1	1	-	-	02572+0253	-47	1	0	0	-	6
02186+3219	-27	1	0	0	5312	6	02396+1300	-42	3	1	1	-	-	02572+0234	-47	1	0	0	2849	6
02186+1620	-41	1	0	0	4105	6	02402+0723	-46	1	0	0	11490	6	02589+3554	-20	1	0	0	7894	5
02197+2801	-31	1	0	0	5085	6	02402+3215	-25	1	0	0	4026	6	02593+1543	-37	2	0	0	-	-
02206+2705	-31	1	0	0	10590	6	02405+3134	-25	1	0	0	4714	5	02599+0200	-47	1	0	0	5181	6

TABLE 2—*Continued*

Name (1)	b (2)	n1 (3)	n2 (4)	n3 (5)	v_h (6)	ref (7)	Name (1)	b (2)	n1 (3)	n2 (4)	n3 (5)	v_h (6)	ref (7)	Name (1)	b (2)	n1 (3)	n2 (4)	n3 (5)	v_h (6)	ref (7)
03004+0411	-45	1	1	0	-	11	03329+0454	-39	1	0	0	6401	5	04129+0832*	-29	3	1	0	-	-
03007+0417	-45	1	0	0	6003	5	03347+0619	-38	3	1	1	9930	1	04130+0840*	-29	3	1	0	-	-
03015+0901*	-42	3	1	0	-	-	03352+1202	-34	3	1	1	6417	6	04133+0803	-29	1	0	0	1592	5
03017+0724	-43	3	1	1	7800	7	03357+2304	-26	3	1	1	16700	11	04134+1333	-26	3	1	1	-	8
03020+2336	-30	3	0	0	15839	6	03359+1523	-31	3	0	0	10590	6	04137+1217	-27	3	1	1	-	-
03025+1910	-33	1	0	0	13334	4	03371+1046	-34	2	1	0	10699	7	04139+2737	-16	3	1	1	5298	1
03027+0211	-46	1	1	0	-	8	03377+1008*	-35	3	1	0	-	-	04139+0238	-32	1	0	0	3349	5
03028+2200	-31	1	0	0	4258	6	03378+1734	-29	1	0	0	9936	5	04140+0103	-33	3	1	0	22230	6
03032+3549	-19	1	0	0	8225	6	03400+2327*	-25	3	1	0	-	-	04141+0008	-34	3	1	1	10050	6
03042+0620	-43	3	1	0	-	-	03403+1013	-34	3	1	1	-	-	04144+1020	-28	3	0	0	7500	6
03056+2034	-32	1	0	0	8225	5	03405+3333*	-17	3	1	0	-	-	04147+0218	-32	1	0	0	3245	5
03058+0154	-46	1	0	0	6101	5	03409+2346	-24	3	1	1	-	-	04147+1809	-23	3	1	1	-	-
03059+0622	-43	3	1	0	-	-	03412+0622	-36	1	1	1	8858	9	04149+0125	-33	1	1	1	4890	1
03061+3143	-23	3	1	0	-	8	03415+2504*	-23	3	1	0	-	-	04150+3528	-11	3	1	1	15199	9
03061+1959	-32	3	1	1	10564	1	03421+2333*	-24	3	1	0	-	-	04151+0126	-33	1	0	0	4927	6
03067+1818	-33	1	0	0	10730	5	03437+3140*	-18	3	1	0	-	-	04154+1755	-23	3	1	1	16659	7
03073+3453	-20	1	0	0	6561	6	03446+1221	-32	2	0	1	-	-	04161+0306	-32	3	0	0	7495	6
03079+0018	-47	3	0	1	14236	1	03459+1259*	-31	3	1	0	6283	1	04165+1002*	-27	3	1	0	-	-
03081+1635	-35	2	0	0	-	11	03475+1238*	-31	3	1	0	-	-	04172+0158	-32	1	0	0	4214	6
03087+0107	-46	1	0	0	9656	6	03497+3526	-14	1	0	0	5802	5	04175+0005	-33	1	0	0	5165	6
03106+3549	-19	3	0	1	-	-	03505+1701	-28	3	1	1	-	-	04187+0042	-32	3	1	0	12300	11
03116+2523	-27	1	0	1	9663	1	03514+1546	-28	1	0	0	6662	5	04191+1523*	-24	3	1	0	-	-
03117+3537	-19	3	1	1	-	-	03515+1513	-29	3	1	1	8433	1	04192+2650	-16	2	2	1	-	8
03118+1916*	-32	3	1	0	-	8	03521+0028	-38	3	1	1	45622	7	04192+0355	-31	1	0	0	7434	6
03119+1448	-35	3	1	1	23006	7	03550+0609	-34	3	1	0	5388	1	04203+1415	-24	3	1	1	14050	1
03125+0119	-45	3	0	0	7200	6	03552+0656	-33	3	1	1	-	-	04210+1303	-25	3	1	0	7766	1
03131+3256	-21	3	1	1	-	-	03578+1955	-24	2	0	1	-	8	04213+3345	-11	1	2	0	5485	2
03131+0858	-40	3	1	1	7858	1	03589+3143A	-16	3	1	1	5180	1	04214+3112	-13	3	1	1	10091	10
03144+0327	-43	1	0	1	890	11	03589+3143B	-16	3	1	1	5454	1	04226+0944	-26	3	1	1	5828	1
03144+0104	-45	1	1	0	7098	7	03598+1656	-26	3	1	1	-	-	04232+1436*	-23	3	1	0	-	11
03147+2942*	-23	3	1	0	-	-	04012+2159	-22	1	0	0	6361	6	04238+2935	-13	3	1	1	7881	1
03152+1135	-37	3	1	1	-	8	04014+3340	-14	1	2	0	5240	2	04239+2449	-17	3	1	1	-	-
03178+0358	-42	1	0	0	8985	6	04017+0638	-32	3	1	1	5644	1	04248+1110*	-25	3	1	0	-	-
03188+1322	-35	1	1	0	8497	1	04020+2507	-20	1	0	0	7166	5	04250+1037	-25	3	1	1	5460	1
03211+1600	-33	1	1	1	11620	4	04023+2114	-23	3	1	1	8934	6	04251+2132	-18	1	0	0	2407	5
03222+1617	-33	3	1	1	12110	1	04026+3035	-16	3	1	1	-	-	04254+0702	-27	3	1	1	-	8
03228+2624*	-25	3	1	0	-	-	04030+3055	-16	3	1	1	-	-	04261+0738	-27	1	1	1	-	11
03235+3004	-22	2	0	1	-	-	04033+3108	-15	1	2	0	9099	2	04271+1807	-20	2	0	0	-	-
03238+1748	-31	3	1	1	11599	1	04050+0350	-33	1	0	0	5298	5	04275+3531	-9	2	0	0	-	-
03250+1606	-32	3	1	1	7176	1	04050+2309	-21	1	0	0	6278	6	04278+1603	-21	2	0	0	-	-
03250+0856	-38	3	1	1	7197	1	04064+0831	-30	1	0	0	3482	5	04282+0526	-28	1	0	0	4640	5
03254+3050	-21	3	1	1	-	-	04082+1351	-27	3	1	1	15831	1	04284+0731	-27	1	0	0	2897	6
03275+1535	-32	3	1	1	7917	1	04089+1233	-27	3	1	1	-	-	04285+0824	-26	1	1	1	4343	1
03280+3517	-17	1	0	0	4479	5	04101+2450	-19	2	0	1	-	-	04287+0803	-26	1	0	0	4021	6
03292+2810	-22	3	1	1	-	-	04102+0214	-33	1	0	0	5001	5	04288+2250*	-17	3	1	0	-	-
03309+2404	-25	2	0	1	-	-	04104+2724	-17	1	0	0	4004	5	04288+2417	-16	2	2	1	-	-
03312+0906	-36	3	1	1	5626	1	04105+2541	-18	3	1	1	6546	1	04291+3306	-10	1	2	0	5422	2
03315+0055	-42	3	0	0	14372	6	04110+3324	-13	3	1	1	-	10	04293+0640	-27	1	1	1	8181	1
03319+1325	-33	3	1	1	10042	1	04112+2432	-19	1	1	1	8552	1	04303+0932	-25	3	1	1	5465	1
03325+2823	-22	3	1	1	-	-	04125+2902	-15	2	0	0	-	-	04309+1144	-24	3	1	1	4370	1

TABLE 2—*Continued*

Name (1)	b (2)	n1 (3)	n2 (4)	n3 (5)	v_h (6)	ref (7)	Name (1)	b (2)	n1 (3)	n2 (4)	n3 (5)	v_h (6)	ref (7)	Name (1)	b (2)	n1 (3)	n2 (4)	n3 (5)	v_h (6)	ref (7)
04316+3427	-9	3	0	1	-	-	05071+0725	-19	1	0	0	5689	5	05361+1532	-8	1	2	0	5820	2
04320+2505	-15	2	2	0	3743	2	05076+0050	-22	1	0	0	8697	5	05364+0706	-13	2	2	0	-	-
04324+1705	-20	1	0	0	3290	6	05081+0020	-22	1	0	0	2821	5	05379+2231	-4	3	2	0	-	-
04332+1910	-19	3	1	1	-	-	05083+2441	-9	3	1	0	6930	2	05383+0611	-13	3	2	0	7598	2
04333+2442	-15	2	2	0	4866	2	05085+2036	-11	3	2	1	9490	7	05385+2355	-3	3	1	0	-	-
04346+0926	-24	1	0	0	8368	6	05086+1659	-13	1	0	0	5176	5	05388+3409	2	3	0	0	-	-
04359+1844	-18	1	0	0	3290	5	05094+0524	-19	1	0	0	4415	5	05389+1828	-6	1	2	0	4574	2
04363+1125	-23	1	1	1	7851	1	05100+0614	-19	3	1	1	5932	1	05395+3537	3	3	0	0	-	-
04372+1225*	-22	1	1	0	7931	1	05102+0239	-20	1	0	0	8347	6	05399+2631	-2	3	0	0	-	-
04380+0024	-29	1	1	1	4516	1	05113+0627	-18	3	1	1	8930	1	05403+3038	1	3	1	0	-	-
04390+2024	-17	3	0	0	4944	6	05119+1318	-14	3	1	1	-	8	05404+2913	0	3	0	0	-	-
04391+3351	-8	2	1	1	-	-	05120+0145	-21	3	1	0	-	-	05406+2305	-3	2	0	0	-	-
04403+0031	-28	1	0	0	4633	5	05125+0612	-18	1	1	1	4491	1	05406+3020	0	3	0	0	-	-
04406+2852	-11	3	2	0	6501	2	05129+0708	-18	1	1	0	8909	6	05408+1636	-7	3	2	0	9083	10
04414+0844	-23	1	0	0	9186	11	05135+1534	-13	3	2	0	6147	2	05418+1242	-9	2	0	0	-	-
04416+2809	-11	3	1	1	3403	1	05135+0603	-18	1	0	0	9285	5	05419+1645	-7	1	0	0	5403	6
04416+1215	-21	3	1	1	-	-	05145+3023	-4	3	2	0	6266	10	05420+0212	-14	3	1	1	-	-
04432+1953*	-16	3	1	0	-	-	05155+0707*	-17	3	1	0	-	-	05430+3154	2	3	1	1	7422	1
04438+0324	-26	1	0	0	4265	6	05163+0435	-18	3	1	1	-	8	05431+3039	1	3	0	0	-	-
04444+2353	-14	1	2	0	3762	2	05164+1649	-12	1	0	0	6959	5	05437+3417	3	2	0	0	-	-
04470+0314	-25	1	0	0	8337	6	05167+0116	-20	1	0	0	8186	5	05444+3520	4	2	0	0	-	-
04479+0616	-23	2	0	1	-	-	05174+0326	-19	3	1	1	-	8	05447+2400	-2	3	1	1	-	-
04479+0555	-23	1	0	0	4613	5	05175+0547	-17	1	1	0	8570	6	05452+2654	-1	3	0	0	-	-
04479+0846	-22	3	1	0	-	-	05184+0357	-18	1	0	0	4145	5	05452+2937	1	3	1	0	7628	3
04482+1250	-19	3	1	1	8514	9	05187+0450	-18	1	1	0	4266	5	05459+1910	-4	2	2	0	5769	2
04490+0525	-24	3	0	0	4561	6	05187+1519	-12	3	2	1	-	8	05461+3148	2	3	0	0	7957	10
04502+0258	-25	1	0	0	4454	5	05189+1700	-11	3	2	0	6537	2	05464+1749	-5	1	2	0	4556	2
04503+0114	-25	1	0	0	8208	6	05192+0317	-18	1	1	1	4485	1	05466+1738	-5	1	2	0	4405	7
04513+0104	-25	1	1	1	6889	1	05206+1911	-9	3	2	0	9760	7	05468+2007	-4	3	2	0	-	-
04521+2531	-11	3	2	1	-	8	05209+2126	-8	3	2	0	5693	2	05472+1336	-7	1	1	0	7596	10
04528+0044	-25	3	1	0	-	-	05232+3525	0	3	0	0	-	-	05478+2925	1	3	0	0	8742	10
04535+0204	-24	1	0	0	4550	5	05235+1534	-11	3	2	1	6655	9	05492+1611	-5	3	2	0	4037	2
04536+1057	-20	2	0	1	-	8	05256+1120	-13	3	1	1	-	-	05497+1246	-7	3	2	0	3644	2
04547+3454	-5	3	1	0	-	10	05273+1045	-13	3	1	1	7605	1	05502+0103	-13	3	1	1	-	-
04559+1644	-16	3	1	1	20792	11	05298+0011*	-17	3	1	0	-	-	05518+1509	-5	1	2	0	2761	2
04565+0454	-22	1	0	0	4723	6	05314+1304	-11	3	1	1	-	-	05518+2814	1	3	0	0	9119	10
04566+0532	-22	1	0	0	4691	6	05316+0246	-16	1	1	1	4016	1	05524+2841	2	3	0	0	7470	10
04576+0912	-20	3	1	1	10822	9	05318+3225	0	3	1	1	-	-	05537+1331	-6	3	1	1	7731	1
04576+1010	-19	3	1	1	14240	9	05321+3205	0	3	1	0	2720	1	05539+2142	-2	3	1	0	-	-
04585+0729	-20	1	0	0	15510	6	05327+1023	-12	3	1	1	-	-	05539+2159	-1	3	0	0	-	-
04586+1201	-18	3	1	1	-	8	05327+0251	-16	3	1	1	5766	1	05541+1606	-4	3	2	0	8246	6
05008+0035	-24	1	0	0	4196	5	05328+0837	-13	3	2	1	10280	10	05541+1149	-6	3	0	0	3663	10
05009+0436	-21	1	0	0	8908	6	05331+3230	0	3	1	0	-	-	05546+1640	-4	2	2	0	-	10
05010+0130	-23	1	0	0	4633	5	05339+0825	-12	3	2	1	11140	1	05546+3107	3	3	0	0	-	10
05016+0434	-21	1	0	0	10695	5	05344+2256	-5	2	0	0	-	-	05555+0909	-7	3	1	0	-	-
05016+2324	-11	3	2	1	-	8	05345+2657	-3	3	1	1	-	-	05556+0144	-11	3	1	1	-	-
05017+2639	-9	2	2	0	-	-	05345+3505	2	3	0	0	-	-	05565+1022	-7	3	1	0	-	-
05028+2135	-12	3	1	1	5120	1	05346+0837	-12	3	1	1	10280	10	05569+3544	6	3	0	0	2990	6
05061+1007	-17	2	0	0	-	-	05347+0947	-12	3	1	0	5084	1	05571+1201	-6	3	1	0	-	-
05066+0844	-18	3	1	1	10949	1	05347+2342	-4	3	1	0	-	-	05574+3037	4	3	0	0	8721	10

TABLE 2—*Continued*

Name (1)	b (2)	n1 (3)	n2 (4)	n3 (5)	v_h (6)	ref (7)	Name (1)	b (2)	n1 (3)	n2 (4)	n3 (5)	v_h (6)	ref (7)	Name (1)	b (2)	n1 (3)	n2 (4)	n3 (5)	v_h (6)	ref (7)
05576+2501	1	3	0	0	-	-	06244+0405	-4	3	2	0	-	-	06521+2417	12	1	0	0	4670	5
05586+3056	4	3	0	0	-	-	06252+2419	6	3	2	0	12301	7	06522+1955	10	3	0	0	19495	10
05586+1247	-5	3	1	0	-	-	06269+2421	6	3	2	0	9275	6	06528+0034	1	3	0	0	-	-
05594+1756	-2	2	0	0	-	-	06275+1121	1	3	0	0	-	-	06532+1539	8	3	0	0	-	8
05595+2201	0	3	0	0	2593	10	06277+1820	4	3	2	0	4082	2	06542+2030	10	1	2	0	4989	2
06006+2735	3	3	1	0	5142	1	06285+3535	12	1	0	0	7072	10	06546+3548	17	1	1	0	5906	9
06033+0941	-6	3	0	0	-	-	06287+2502	7	3	2	0	9548	2	06547+1107	6	3	0	0	8206	10
06038+1820	-1	3	0	0	-	-	06293+0229	-3	3	0	0	-	-	06549+0912	6	3	0	0	11427	10
06040+2152	1	3	1	1	5829	1	06294+1204	1	2	0	0	-	-	06552+1244	7	1	2	0	8148	7
06048+3416	7	1	0	0	2831	7	06296+2358	7	3	0	0	-	-	06558+1244	7	1	2	0	8050	2
06050+2341	2	3	0	0	-	-	06298+1037	1	2	0	0	-	-	06560+1021	6	3	0	0	-	10
06071+0440	-7	3	1	0	-	8	06305+2104	6	1	2	0	5461	2	06582+0739	6	3	0	0	-	-
06072+2714	4	3	2	0	-	-	06311+1210	2	3	0	0	-	3	06591+0459	5	1	0	0	3550	6
06073+0915	-5	3	2	0	-	-	06314+1656	4	3	2	0	-	-	07003+0144	3	3	0	0	15259	9
06074+3539	8	1	0	0	5740	10	06324+1501	3	1	2	0	3790	2	07005+3415	17	1	0	0	8214	9
06098+0642	-6	3	2	0	3782	2	06339+1921	6	3	1	0	5312	1	07019+1623	10	1	0	0	12628	10
06102+1537	-1	3	0	0	-	-	06342+2708	9	3	0	0	-	8	07021+1033	8	2	0	0	10908	10
06108+2300	3	3	0	0	-	-	06343+0425	-1	3	0	0	-	-	07021+2948	16	3	1	1	26831	9
06116+2237	3	3	0	0	-	-	06344+0213	-2	3	0	0	-	-	07024+2103	12	3	2	0	-	8
06125+0012	-8	3	0	0	2339	6	06353+0218	-2	3	0	0	-	-	07028+1745	11	3	0	0	-	10
06147+1330	-1	3	0	0	-	-	06367+1043	2	3	0	0	-	-	07032+3514	18	3	0	0	-	-
06154+2257	4	3	0	0	-	-	06375+3338	13	1	1	0	5137	7	07034+2109	13	3	0	0	12663	10
06154+1524	0	3	0	0	-	-	06377+1535	5	2	2	0	-	-	07038+0221	4	3	0	0	5528	10
06155+1621	0	3	1	1	-	-	06387+0116	-2	3	0	0	-	-	07048+1600	11	3	1	1	-	10
06159+0440	-5	3	1	0	-	-	06393+3117	12	3	1	0	-	-	07051+1515	11	1	2	0	2208	2
06165+1826	2	3	0	0	5475	3	06397+0506	0	3	0	0	-	-	07063+0700	7	1	2	0	5973	2
06173+2506	5	2	2	0	6080	10	06416+3521	14	1	1	0	-	8	07073+3430	19	1	0	0	4918	5
06177+2355	4	2	0	0	-	-	06416+0242	0	3	0	0	-	-	07079+0632	7	1	0	0	3569	10
06178+1133	-2	2	0	0	-	-	06423+1432	5	3	0	0	14888	-	07080+2559	16	1	0	0	7565	6
06179+0810	-3	3	0	0	-	-	06439+0221	0	3	0	0	-	-	07084+2915	17	1	0	0	4902	5
06183+0837	-3	3	0	0	-	-	06442+3223	13	1	1	1	5079	1	07092+0541	7	3	0	0	10192	10
06186+2711	6	1	2	0	6308	2	06443+2925	12	1	1	0	5212	7	07092+2609	16	1	1	1	7711	1
06188+1026	-2	3	0	0	7455	10	06445+0544	2	3	0	0	-	-	07107+3521	20	1	0	0	4705	5
06189+1909	2	3	2	0	5532	2	06460+0340	1	3	0	0	-	-	07112+0750	9	1	0	0	8718	10
06193+0130	-6	2	0	0	-	10	06468+0600	2	2	0	0	-	-	07117+0806	9	3	0	0	9114	9
06195+2256	4	2	0	0	-	-	06472+2858	13	3	1	0	-	8	07119+1704	13	1	2	0	4909	2
06197+0432	-4	3	2	0	2947	2	06474+3110	14	3	0	0	5428	10	07120+1428	12	2	2	0	8312	7
06209+2527	6	2	2	0	-	-	06478+3335	15	1	1	0	5090	5	07125+2615	17	1	1	0	9145	7
06213+0444	-4	1	2	0	2887	2	06482+1258	6	1	2	0	3951	2	07129+3301	19	1	0	0	7242	5
06215+0827	-2	3	0	0	-	-	06486+3002	13	3	0	0	5201	10	07131+0948	10	3	2	0	8192	10
06218+1559	2	3	0	0	4009	10	06486+2052	9	3	0	0	-	8	07133+3404	20	1	0	0	3883	5
06220+0603	-3	3	0	0	-	-	06487+2208	10	3	0	0	43080	9	07135+2956	18	1	0	0	3213	5
06224+3041	8	1	0	0	-	8	06494+1518	7	1	0	0	4531	6	07141+0751	9	1	0	0	-	11
06226+0908	-2	2	0	0	-	-	06498+2741	13	1	2	0	5106	2	07141+3410	20	1	0	0	3960	5
06227+0938	-1	3	0	0	-	-	06501+2222	10	1	0	0	4880	10	07142+1732	13	3	1	1	-	10
06232+0634	-3	3	0	0	-	-	06505+0010	0	3	0	0	-	-	07146+2326	16	1	2	0	2270	2
06232+2806	7	2	2	0	13598	10	06508+2330	11	3	1	1	18523	6	07148+1246	12	3	0	0	-	10
06232+2004	4	3	2	0	-	-	06509+0312	2	2	0	0	-	-	07150+0802	9	1	0	0	5490	10
06235+2543	6	3	2	0	11418	10	06514+0845	5	3	2	0	6370	2	07170+3230	20	3	1	1	7463	7
06244+0336	-4	3	0	0	-	-	06515+1141	6	3	0	0	7857	10	07176+2637	18	1	0	0	10463	9

TABLE 2—*Continued*

Name (1)	b (2)	n1 (3)	n2 (4)	n3 (5)	v_h (6)	ref (7)	Name (1)	b (2)	n1 (3)	n2 (4)	n3 (5)	v_h (6)	ref (7)	Name (1)	b (2)	n1 (3)	n2 (4)	n3 (5)	v_h (6)	ref (7)
07194+1723	15	1	1	0	2528	2	07521+1435	21	1	0	0	-	11	08201+2801	31	3	0	0	50215	9
07199+2033	16	3	0	0	-	11	07523+2652	25	1	0	0	4626	5	08202+0343	22	1	0	0	3983	5
07200+3235	20	1	0	0	4529	6	07538+1807	22	1	0	0	-	8	08206+2130	29	1	0	0	5323	5
07200+0130	8	2	0	0	-	10	07538+1703	22	1	0	0	-	8	08208+2816	32	3	0	0	-	8
07201+2218	17	1	0	0	5367	5	07541+0736	18	1	0	0	4610	5	08209+1755	28	3	1	1	18258	9
07208+0242	8	1	0	0	1363	6	07566+3325	28	1	0	0	5888	5	08209+1139	26	3	0	0	-	8
07219+2725	19	1	0	0	7613	6	07567+3557	29	1	0	0	5253	7	08214+0713	24	3	0	0	19516	9
07220+2352	18	1	0	0	5500	5	07568+1531	22	1	0	0	4623	5	08222+1341	27	1	0	0	-	11
07223+0004	7	3	0	0	9672	10	07568+2331	25	1	0	0	8749	6	08228+1136	26	3	0	0	-	8
07224+3003	20	1	0	0	5671	6	07572+0544	18	1	0	0	2618	5	08234+1054	26	3	1	1	19666	9
07233+3355	22	1	0	0	7786	6	07577+2738	27	1	0	0	5206	6	08235+0445	23	1	0	0	-	6
07235+2310	18	1	0	0	-	11	07581+1648	23	3	1	1	-	8	08237+0305	22	1	0	0	-	11
07238+2821	20	3	1	1	11589	1	07590+1815	23	3	1	1	-	-	08242+0735	25	3	1	1	9411	1
07240+0324	9	3	0	0	9480	10	07594+2008	24	3	1	1	-	8	08245+1726	29	1	0	0	5934	5
07244+1944	17	1	0	0	9907	5	07595+2734	27	1	1	0	5228	5	08247+2138	30	1	0	0	4330	6
07249+1303	14	3	1	1	2193	10	08001+2331	26	1	0	0	4702	6	08249+0303	23	1	0	0	-	8
07259+2041	17	1	0	0	4464	5	08002+3336	29	1	0	0	11730	6	08254+0510	24	3	0	0	9144	9
07261+1318	14	3	1	1	-	-	08003+0734	19	3	0	0	-	-	08268+2235	31	3	0	0	-	-
07299+0536	12	3	1	1	14853	1	08004+2514	26	1	0	0	8300	6	08269+0122	22	1	0	0	75	11
07306+2533	20	3	0	0	20408	11	08012+0850	20	1	0	0	4932	6	08276+1558	29	3	0	0	-	-
07317+3123	22	1	0	0	4680	5	08040+2716	28	1	0	0	12240	6	08292+2243	32	1	0	0	4750	6
07318+3255	23	1	0	0	4678	5	08042+0808	20	1	0	0	4603	5	08303+2942	34	1	0	0	2094	5
07324+1232	15	3	0	0	-	8	08044+2516	27	1	0	0	-	8	08319+0150	24	1	0	0	4212	6
07326+1149	15	1	2	0	4984	2	08048+0439	19	1	0	0	9125	6	08322+2838	34	1	0	0	2135	6
07338+1138	15	3	1	1	18468	9	08050+1757	25	1	0	0	5029	5	08323+3003	34	3	1	1	-	-
07340+0300	11	3	2	1	5140	7	08056+1228	23	3	1	1	10068	1	08325+2512	33	1	0	0	-	8
07342+1342	16	1	0	0	4725	5	08066+0025	17	1	0	0	-	5	08327+2855	34	1	0	0	7621	6
07343+3543	24	1	0	0	3994	5	08071+0509	20	3	0	0	15600	6	08332+2814	34	1	0	0	3475	6
07372+0637	14	3	1	1	12270	1	08076+0805	21	1	0	0	-	11	08340+1550	30	3	1	1	23414	7
07373+3420	24	1	0	0	4525	5	08082+2521	28	1	0	0	4099	5	08345+2852	35	1	0	0	3474	5
07400+0045	12	3	0	0	-	8	08087+0347	19	1	0	0	3944	5	08351+1257	29	1	0	0	-	11
07405+2303	21	1	0	0	7261	5	08091+1930	26	1	0	0	8533	5	08355+1945	32	1	0	0	4527	9
07408+3311	25	1	0	0	16428	9	08097+2630	29	1	0	0	6301	5	08365+0444	26	1	0	0	-	6
07410+2922	24	1	0	0	4750	6	08111+2401	28	1	0	0	6048	5	08368+2319	34	1	0	0	7503	7
07423+0003	12	1	0	0	8524	10	08113+2130	27	1	0	0	3373	5	08389+0509	27	1	0	0	1939	5
07424+1231	18	3	1	1	-	8	08122+0505	21	3	0	0	30878	9	08405+1315	31	1	0	0	2068	5
07424+0803	16	1	2	0	5050	2	08130+2321	28	1	0	0	4286	5	08409+3453	37	1	0	0	4244	5
07433+1047	17	1	0	0	-	11	08132+1629	26	3	0	0	-	-	08423+3436	38	1	0	0	7704	6
07439+2804	24	1	0	0	8254	6	08143+3536	32	1	0	0	2400	5	08428+1954	34	3	0	0	-	-
07439+3036	25	1	0	0	4246	6	08144+2150	28	1	0	0	3565	6	08432+1248	31	1	0	0	4111	5
07449+0050	13	3	0	0	10349	10	08145+0050	19	3	1	1	-	8	08452+1753	34	1	0	0	-	8
07450+3427	26	1	0	0	4415	5	08153+1541	26	3	0	0	13341	9	08470+3515	39	1	0	0	2306	6
07451+2821	24	1	0	0	8262	6	08161+2156	29	1	0	0	4510	6	08474+1232	32	1	0	0	-	11
07464+0507	15	3	0	0	-	-	08166+0357	21	1	0	0	-	6	08474+1813	34	3	0	0	-	8
07466+3405	26	1	0	0	4794	5	08166+2116	28	1	0	0	5488	5	08481+1042	31	3	0	0	-	-
07468+3436	26	1	0	0	-	8	08168+2211	29	1	0	0	3591	6	08483+0231	28	3	0	0	-	-
07469+3051	25	1	0	0	4282	5	08169+0448	22	1	0	0	4073	5	08484+2521	37	3	1	1	-	8
07509+1328	20	1	0	0	-	11	08178+1931	28	1	0	0	5732	6	08502+0930	31	1	0	0	8822	7
07516+1656	21	1	0	0	13891	11	08188+0319	21	1	0	0	2684	5	08507+3520	39	1	0	0	16560	6
07517+0435	16	1	0	0	4114	5	08195+0325	22	1	0	0	4131	5	08510+0055	27	3	1	1	-	-

TABLE 2—*Continued*

Name (1)	b (2)	n1 (3)	n2 (4)	n3 (5)	v_h (6)	ref (7)	Name (1)	b (2)	n1 (3)	n2 (4)	n3 (5)	v_h (6)	ref (7)	Name (1)	b (2)	n1 (3)	n2 (4)	n3 (5)	v_h (6)	ref (7)
08512+2727	38	3	0	0	-	-	09206+1723	41	3	0	0	-	-	09402+2124	47	1	0	0	4940	5
08532+0059	28	1	0	0	-	6	09214+2830	45	1	0	0	6518	6	09406+0038	38	1	0	0	-	11
08542+1323	34	1	0	0	3978	5	09216+0609	37	1	0	0	3546	6	09406+1018	43	1	0	0	16137	6
08559+1053	33	3	0	0	44700	6	09217+1813	42	1	0	0	8334	9	09411+3455	49	1	0	0	-	11
08561+0629	31	1	0	0	3843	6	09218+2345	44	1	0	0	5996	9	09422+3456	50	1	0	0	12240	6
08570+2047	37	3	1	1	-	8	09222+1633	41	3	1	1	-	8	09426+0738	42	1	0	0	14030	9
08571+3555	41	1	0	0	3081	5	09230+1138	39	1	0	0	3775	5	09428+3454	50	1	0	0	6176	5
08579+0130	29	3	0	0	-	-	09231+3506	46	1	0	0	4800	6	09430+0510	41	1	0	0	3742	5
08579+3447	41	3	0	0	19659	6	09231+0226	35	1	0	0	6959	6	09432+1910	47	3	1	1	16048	7
08584+1356	35	1	0	0	-	11	09232+1935	43	1	0	0	2522	6	09434+0153	39	1	0	0	1872	6
08594+0829	33	1	0	0	2583	5	09235+2220	43	1	0	0	-	11	09435+3508	50	2	0	0	12453	7
08594+1702	36	1	0	0	3830	5	09239+0810	38	1	0	0	2149	5	09438+1141	44	3	1	1	-	-
08596+1443	36	3	1	1	-	11	09244+3039	46	1	0	0	8070	5	09446+0054	38	1	0	0	5927	6
08597+2608	39	1	0	0	2450	5	09250+1230	40	1	0	0	8692	11	09447+3517	50	1	0	0	-	8
09004+1827	37	1	0	0	3368	6	09253+1724	42	1	0	0	4215	5	09456+0244	40	3	1	1	6015	1
09011+2210	39	1	0	0	3108	6	09271+3453	47	1	0	0	-	8	09460+0914	43	1	0	0	-	8
09014+0139	30	3	1	1	9174	1	09273+2945	46	1	0	0	1699	6	09468+0122	39	1	0	0	7559	6
09017+1321	35	1	0	0	-	11	09274+2134	44	1	0	0	-	8	09469+0914	43	1	0	0	-	8
09018+1447	36	1	0	0	14970	6	09275+1941	44	1	0	0	-	8	09471+1255	45	1	0	0	8970	5
09018+1839	37	1	0	0	3428	6	09277+1634	42	1	0	0	8653	5	09471+1039	44	1	0	0	-	8
09020+0835	33	3	0	0	-	8	09282+3014	46	1	0	0	4189	5	09472+0051	39	1	0	0	1879	5
09028+2538	40	1	0	0	2674	6	09294+0839	39	1	0	0	2140	5	09474+1302	45	1	0	0	1440	5
09028+1832	38	1	0	0	8875	5	09297+1508	42	3	0	0	-	8	09477+1259	45	1	0	0	1415	5
09039+0503	32	3	1	1	37474	9	09316+0027	36	1	0	0	4885	6	09484+1557	47	1	0	0	8720	5
09042+2532	40	1	0	0	2832	6	09319+0604	39	1	0	0	5514	5	09487+3551	51	3	0	0	-	11
09045+3309	42	3	1	1	-	8	09321+1030	41	1	0	0	2432	5	09488+2746	50	3	0	0	-	11
09047+1838	38	1	0	0	8728	7	09321+2155	45	1	0	0	3730	5	09492+2928	51	1	0	0	1533	5
09051+3443	42	3	1	1	16069	9	09324+3002	47	1	0	0	8075	5	09495+0119	40	1	0	0	6016	11
09053+3549	42	1	0	0	7174	6	09343+3402	48	3	0	0	-	11	09498+0218	40	3	0	0	-	-
09054+2138	39	1	0	0	2718	5	09343+2003	45	1	0	0	8483	5	09502+1952	49	3	0	0	-	8
09054+2906	41	1	0	0	6436	6	09344+3548	48	1	0	0	-	11	09503+1654	48	1	0	0	1414	5
09065+3319	42	1	0	0	1951	5	09345+3304	48	1	0	0	4362	5	09511+2337	50	1	0	0	3962	5
09070+0722	34	1	0	0	5497	5	09346+2323	46	1	0	0	7509	5	09521+0930	45	1	0	0	1494	6
09109+2329	41	3	0	0	11100	6	09351+0259	38	1	0	0	6981	7	09524+1432	47	1	0	0	7194	6
09115+3020	43	1	0	0	6909	5	09354+0945	41	1	0	0	3338	5	09528+1640	48	1	0	0	3731	5
09119+0819	35	1	0	0	9174	9	09356+0419	39	3	1	1	6864	1	09530+3416	52	1	0	0	-	8
09120+2956	43	1	0	0	6303	5	09357+3457	48	1	0	0	-	11	09534+2727	51	1	0	0	1238	5
09130+2108	41	1	0	0	8959	6	09359+3431	48	1	0	0	-	11	09535+1704	48	1	0	0	3690	5
09135+1756	40	1	0	0	-	11	09362+1715	45	1	0	0	8953	5	09535+1043	46	1	0	0	8944	5
09137+3438	44	1	0	0	1681	5	09362+1329	43	3	1	1	-	8	09539+1552	48	1	0	0	4560	6
09141+2538	42	1	0	0	1531	6	09363+0710	40	1	0	0	4983	5	09549+1424	48	3	0	0	21555	9
09143+0939	37	3	1	1	14251	3	09368+0639	40	1	0	0	-	6	09560+0058	41	3	0	0	19306	9
09145+2610	43	1	0	0	6538	5	09379+1206	43	1	0	0	6663	5	09562+1439	48	1	0	0	3582	5
09160+2628	43	1	0	0	2759	6	09380+0348	39	1	0	0	4932	6	09563+1803	49	1	0	0	-	8
09164+3400	44	1	0	0	5876	9	09380+3457	49	3	1	1	15080	9	09563+3156	52	1	0	0	11400	6
09168+0623	36	3	0	0	24883	11	09380+2541	48	1	0	0	-	11	09583+1142	47	1	0	0	-	11
09168+3308	44	1	0	0	14922	5	09381+2125	46	1	0	0	-	5	09583+2238	51	1	0	0	7615	9
09174+0821	37	3	1	1	8574	9	09388+1138	43	1	0	0	6238	5	09595+1155	47	1	0	0	-	8
09178+3534	45	1	0	0	7477	5	09400+2912	49	1	0	0	8511	5	09598+1925	51	1	0	0	2077	5
09197+2210	43	1	0	0	10180	5	09400+1131	43	3	1	1	-	8							

§ 4.2 to confirm that the newly discovered void between $\alpha = 3^h$ and 4^h is not a selection effect.

2.2. *Observations*

Our goal was to obtain H I spectra of the sources in our candidate sample which were not known to be galaxies at the time of our observations. To this end, we searched the literature for identified galaxies in our sample. Both optical and radio identifications were used.

The 21 cm observations were carried out with the 305 m radio telescope of Arecibo Observatory[1] during sessions between 1993 March and October. The telescope, equipped with the 22 cm dual circular feed and the 2048-channel digital autocorrelator, was operated in the beam switch mode. The pointing accuracy of the telescope was about 20″, the FWHP beam size is about 200″. Since the PSC positions are found to be accurate to ~15″ (*IRAS* Explanatory Supplement 1988), all galaxy candidates were well within the beam at the commanded position of the telescope. A candidate source was usually first observed in the low-velocity range (−400 to 8200 km s^{-1}). If no H I line emission was detected, another spectrum was taken in the high-velocity range (7800 to 16,400 km s^{-1}). Each spectrum was taken with 5 minutes on-source, followed by 5 minutes off-source. After Hanning smoothing, the velocity resolution is ~16 km s^{-1} and the typical rms noise is 1.5 mJy. Flux calibration was achieved to a typical uncertainty of ~15% by using a look-up table of flux scale versus feed central frequency kindly provided by W. Baan. This table has been derived from observations of unresolved continuum radio sources in the standard "PEAK" mode which minimizes the effect of pointing errors.

The 21 cm H I survey of Lu et al. (1990) is similar to the current one, but is limited to $3° < |b| < 16°$ and has a velocity coverage out to 9000 km s^{-1}. Galaxy candidates observed but not detected in this survey were only searched for in our high-velocity window. All the spectra were reduced using the standard GALPAC software package provided by Arecibo Observatory. For detected galaxies, the integral parameters (see § 2.3), including the mean velocity and velocity widths, were derived from their Hanning-smoothed spectra.

2.3. *Results*

A total of 272 candidates were observed up to $v_h \sim 16{,}000$ km s^{-1}, including the 23 sources not in our main sample. We detected 89 galaxies with a signal-to-noise (S/N) ratio of the H I line greater than 3. This includes two galaxies not in our main candidate sample and three galaxies detected in the OFF spectra. In Figure 1, the Hanning-smoothed H I spectra are presented. We give their derived parameters in Table 3 where the columns, from the second one on, are the mean heliocentric velocity in km s^{-1}, taken to be the middle point between the velocities at the flux level 50% of the peak(s) on either side of the profile; velocity widths at 20% and 50% of the mean flux density within the profile; velocity widths at 20%, 50%, and 80% of the peak(s); the integrated H I flux in units of Jy km s^{-1}; and the observed ratio of peak signal-to-noise S/N. The last column marks a few galaxies for which notes are given at the bottom of the table. While all spectra with S/N > 3 were considered to be detections, most of the spectra in Figure 1 have much higher S/N ratios.

[1] The Arecibo Observatory is part of the National Astronomy and Ionosphere Center, which is operated by Cornell University under a cooperative agreement with the National Science Foundation.

3. THE GALAXY SAMPLE AND ITS COMPLETENESS

3.1. *The Sample*

Our final sample of galaxies consists of all sources in Table 2 which are marked as galaxies by a numerical entry in column (7). The total of 717 galaxies includes the three galaxies detected in OFF spectra of observed targets. For $|b| > 10°$, this sample is fairly complete in the sense that most galaxy candidates have been tested whether they are galaxies. For further discussion we define two subsamples: one of 309 galaxies with $b < -10°$ (hereafter referred to as southern-Galactic, or SG, subsample) and one of 318 galaxies with $b > 10°$ (northern-Galactic, or NG, subsample). For $|b| < 10°$, our observational coverage is less complete. The completeness of this third subsample of 90 galaxies is discussed separately below.

Table 4 lists a detailed break down of the number of galaxies in the NG and SG subsamples. Column (2) lists the number of galaxies in each subsample. Column (3) gives the (subsample) percentage of galaxies with velocities currently available. Columns (4) and (5) give the percentages of galaxies observed in our H I surveys in the low-velocity window and in both the velocity windows, respectively, for which velocities are still not available in Table 2. These galaxies are likely to be more distant than the corresponding limiting velocities of our survey. The last two columns list the percentages of galaxies known to have v_h less than 9000 and 16,000 km s^{-1}, respectively.

3.2. *Sample Completeness*

Since the purpose of this work is to investigate the large scale structure hidden behind the ZOA, the completeness of this sample is an important aspect. In this subsection, we first discuss the completeness of the sample drawn from the PSC and then the completeness with which galaxies in that sample were identified.

3.2.1. *Completeness of the Candidate Sample*

The first step in the construction of our sample was the pre-selection of galaxy candidates from the PSC. The completeness of this sample is the ratio of the galaxies which are actually included in our candidate sample to those which satisfy our color and flux criteria. This completeness may depend on the position in the sky if the PSC flux densities are seriously contaminated at low Galactic latitudes or the completeness of the PSC itself depends on spatial position.

Above a few degrees in Galactic latitude, cirrus contamination and source confusion are found to have a small effect on the FIR flux densities of PSC sources (Lu et al. 1990). Indeed, we found that the mean ratio of $f(100)/f(60)$ is about 2.25 for the whole galaxy sample, independent of b.

The PSC may suffer from a severe incompleteness due to the strong lagging of *IRAS* noise estimator at 60 and 100 μm after passage through the Galactic plane (the "shadowing" effect; see *IRAS* Explanatory Supplement 1988), but this incompleteness is limited to within a few degrees of the Galactic plane. On the other hand, there is the possibility that the flux limit of the PSC is higher and/or that the criteria for assigning the flux quality flags are more stringent at lower Galactic latitudes. Such nonhomogeneities of the PSC affect mainly sources with

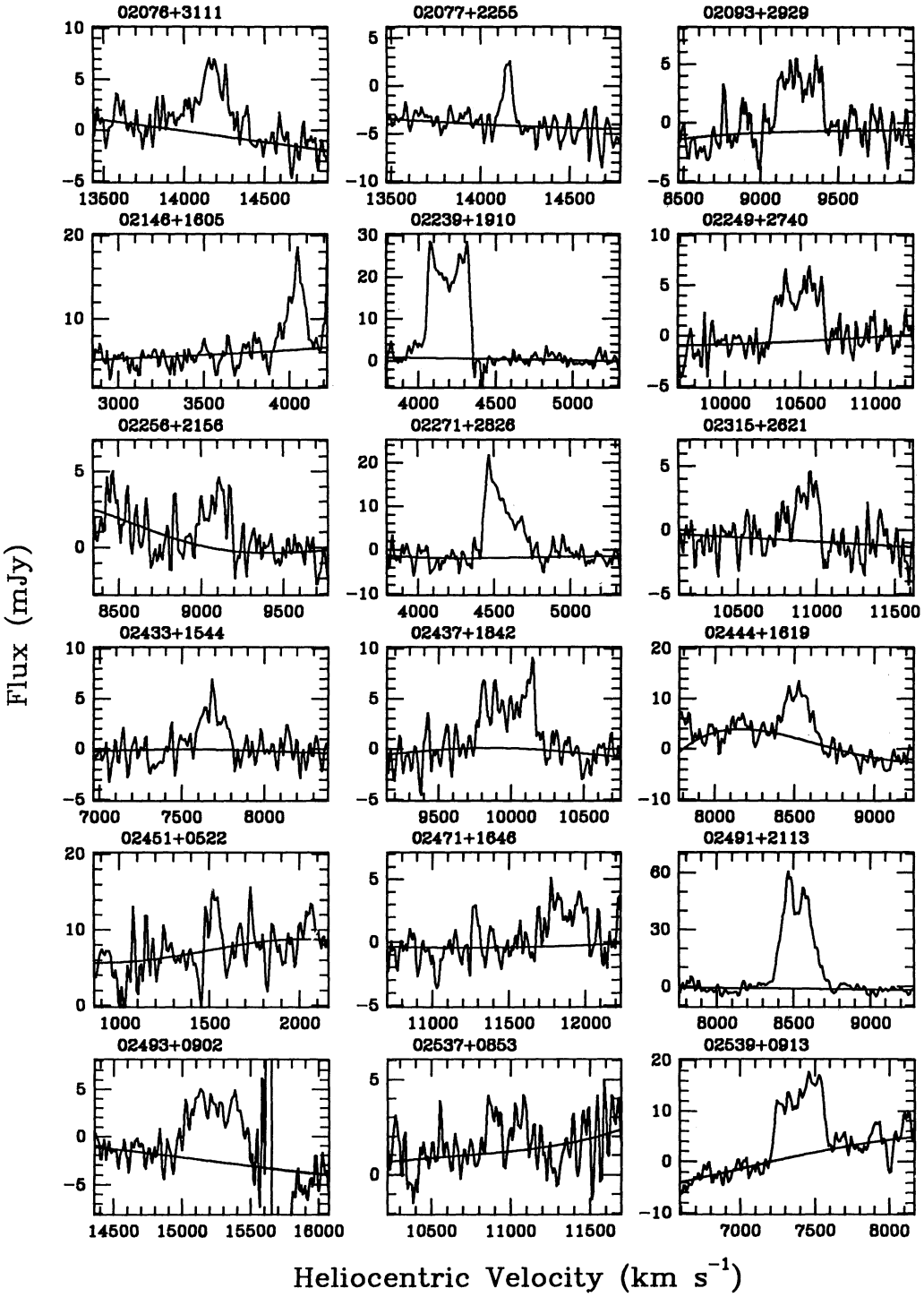

FIG. 1.—H I 21 cm spectra of the detected galaxies in order of right ascension. The ordinate is the H I flux density in mJy, and the abscissa is the heliocentric velocity in km s^{-1}. The three spectra detected in OFF positions (see Table 3) are also shown here.

flux densities near the PSC detection threshold. We investigated the impact of such effects on our sample by comparing the PSC fluxes of our sample galaxies with those of galaxies in a comparison sample at high Galactic latitudes. This "high-latitude" comparison sample (which is described in more detail in § 4.1) contains all 3540 PSC galaxies at $|b| > 35°$, that also satisfy the selection criteria of our sample. For $|b| > 35°$, the above mentioned various kinds of incompleteness are negligible. Figure 2*a* shows the distribution of the *IRAS* 100 μm fluxes of the combined SG and NG galaxy samples as a thick solid line, and that of the comparison sample as a thin solid line. The histogram of the comparison sample has been scaled so that both distributions in Figure 2*a* have the same number of galaxies for $f(100) > 3.5$ Jy. It can be seen that there is a

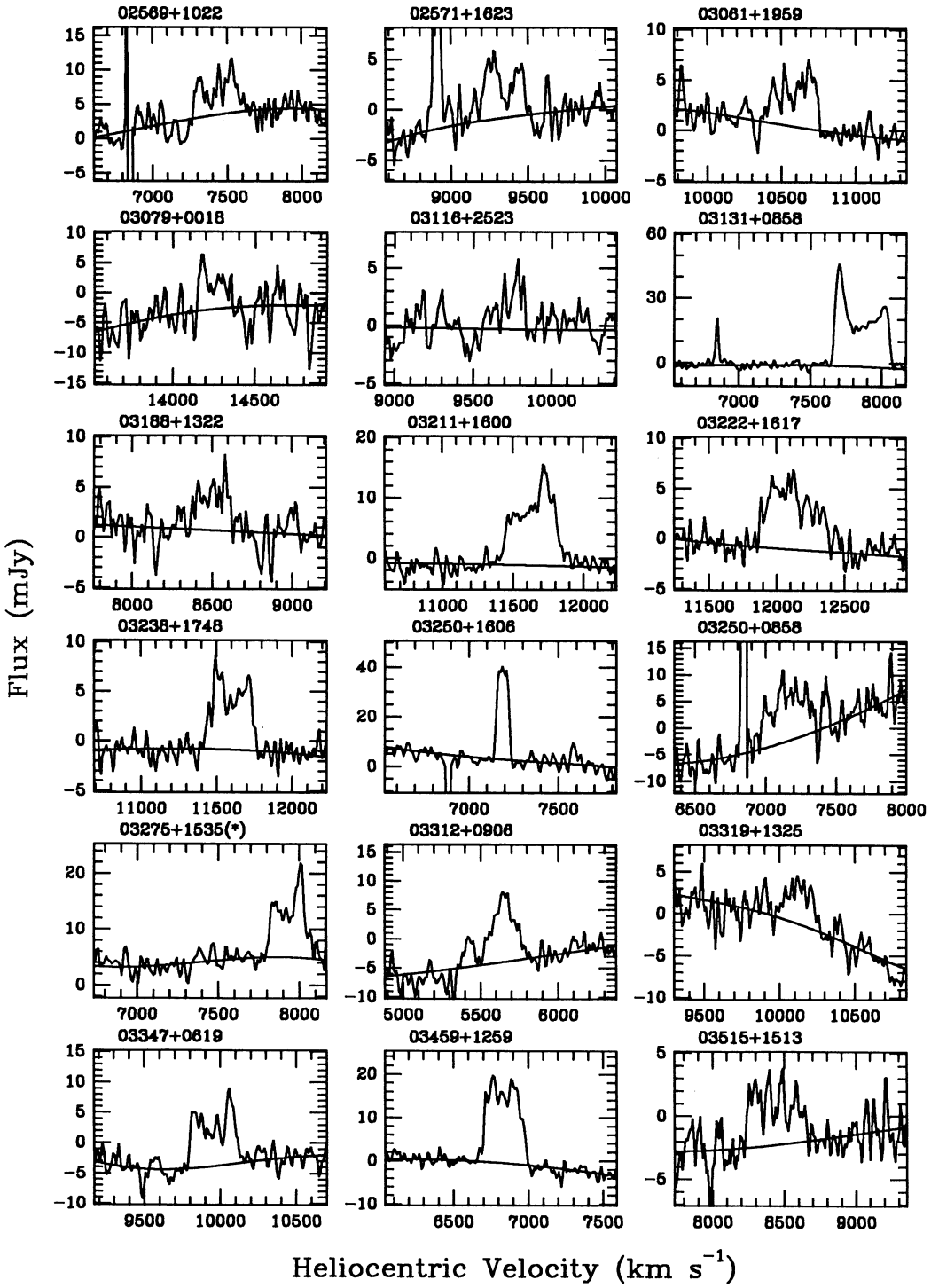

FIG. 1—*Continued*

deficit of galaxies at $f(100) < 2$ Jy in our sample with respect to the comparison sample, while there is no systematic difference between the two histograms for $f(100) > 2$ Jy. The two bins with the lowest fluxes in our galaxy sample contain, respectively, about 40% and 10% fewer galaxies than the corresponding bins in the comparison sample. This suggests that about 60 galaxies are missing in our combined SG and NG subsamples of 628 galaxies as compared to a similar sample constructed at high Galactic latitudes. We therefore conclude that the PSC is less complete for low latitudes in terms of flux limit and/or quality. The fact that 10% of all galaxies which satisfy our selection criteria are not included in our sample due to this effect has to be taken into account if a volume normalization is used to compare this galaxy sample with a high

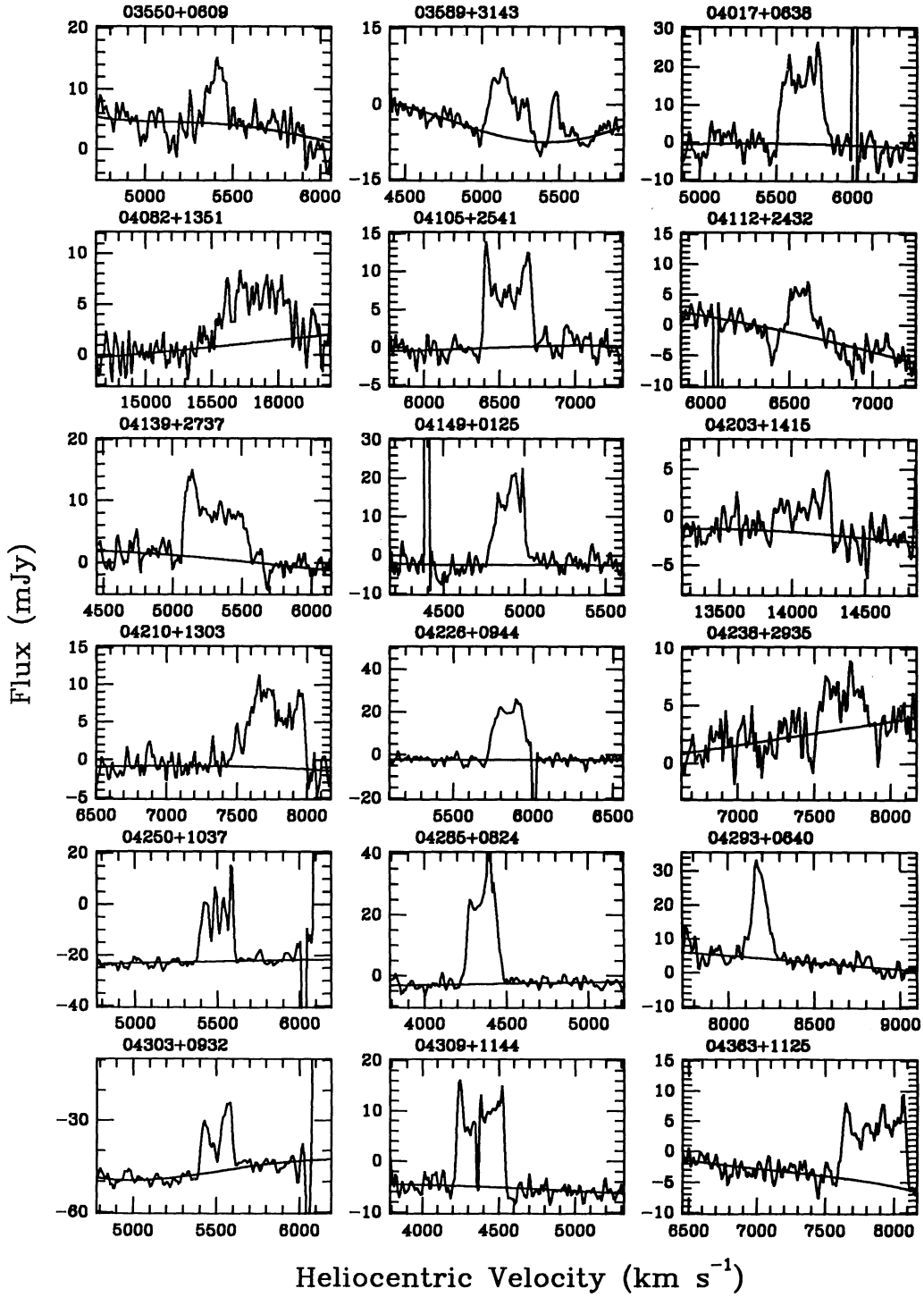

FIG. 1—*Continued*

Galactic latitude sample. However, because of the relatively flat FIR luminosity function of *IRAS* galaxies, this sample incompleteness should only weakly depend on redshift.

Similar to Figure 2*a*, Figure 2*b* compares the flux distributions of the SG (*thick solid histogram*) and NG subsamples. No normalization is used here because the two subsamples occupy roughly the same solid angle on the sky. It shows that much of the lack of low-flux galaxies in Figure 2*a* is due to the SG sample, which includes the Orion-Taurus region with $b < -10°$. The number of galaxies apparently missing in the SG sample (relative to the NG sample) is 25, or ~4% of the size of the combined SG and NG subsamples. It can also be seen in Figure 2*b* that there is no significant difference between the two subsamples for $f(100) > 2$ Jy. Except for $|b| < 10°$ these two subsamples also divide the survey area into regions of the least and most Galactic obscuration (see § 4.1). Thus, the

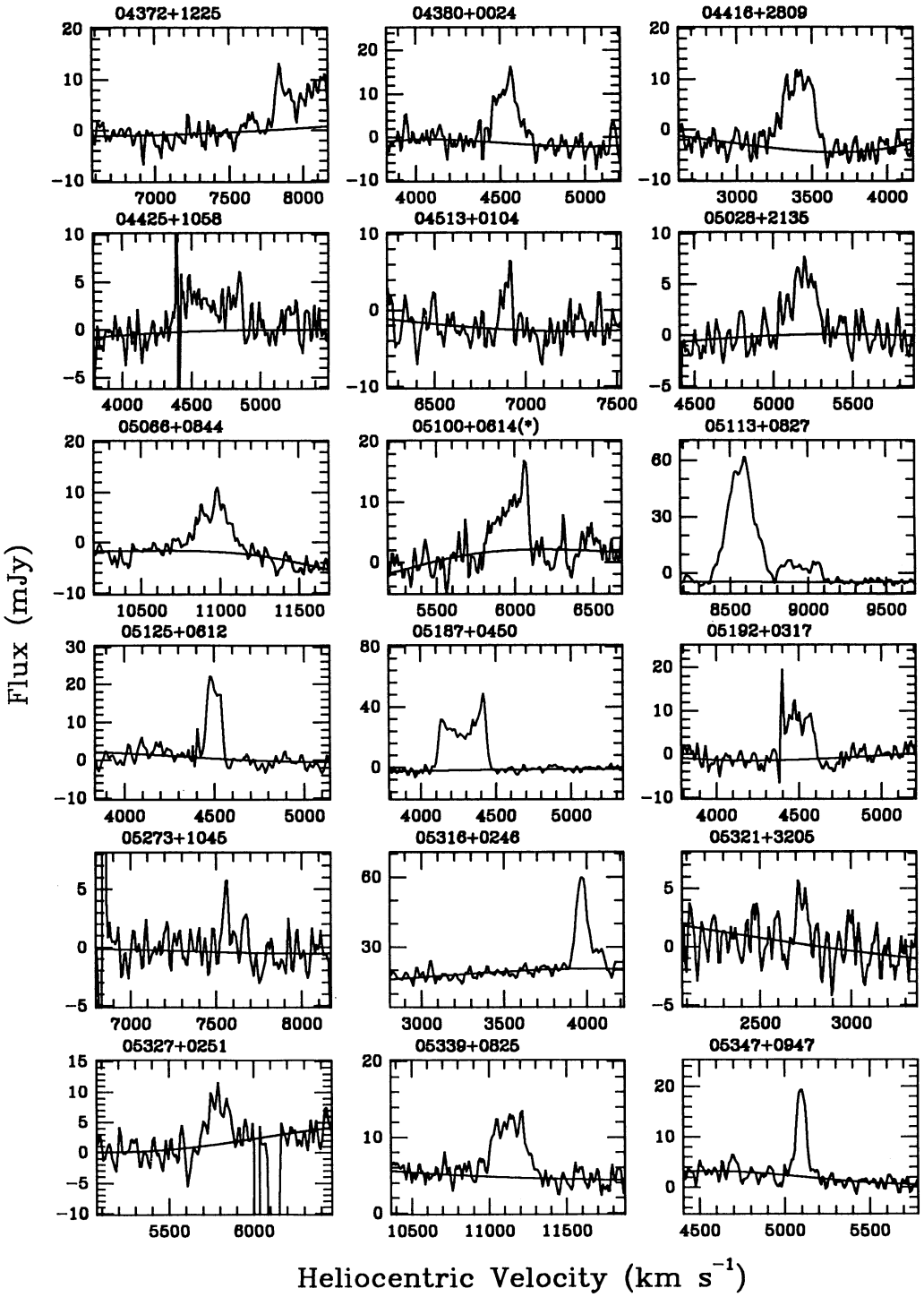

FIG. 1—*Continued*

above 4% differential incompleteness between the two subsamples can be regarded as an upper limit on the nonuniformity between any two directions in our survey area of $|b| > 10°$.

Since the galaxy identification in our candidate sample is still not quite complete for $|b| < 10°$ (see § 3.2.2 below), we cannot quantitatively assess the size of the above PSC incompleteness for this region. The fact that galaxy detection rate in the complete survey of Lu et al. (1990) varies only slowly down to $|b| \sim 3°.5$ suggests that this PSC incompleteness does not increase drastically even for $5° \lesssim |b| < 10°$ in our survey area. Nevertheless, we will exclude the region of $|b| < 10°$ for most of the statistical analysis below.

3.2.2. *Completeness of the* H I *Surveys*

The completeness of our H I surveys as a function of heliocentric velocity v_h depends on (1) the fraction of candidate sources which are either confirmed or ruled out to be galaxies

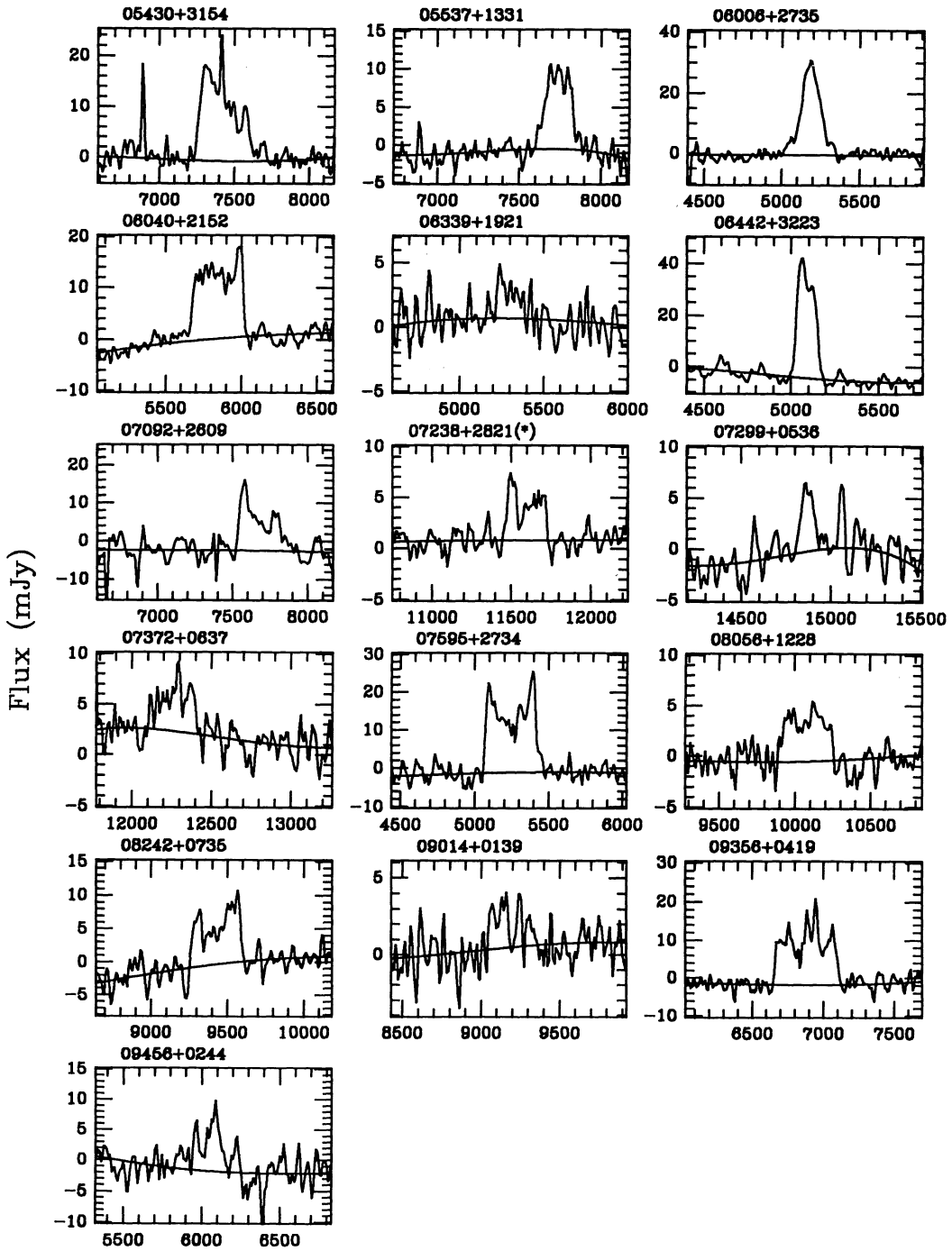

FIG. 1—*Continued*

with redshifts smaller than the one considered, and (2) the fraction of the selected galaxies whose H I emission is below the sensitivity of the H I survey. A high degree of completeness is necessary to avoid nonuniformities in the final sample as we accepted galaxy identifications from other surveys.

The degree of completeness (1) is illustrated in Figure 3 as a function of Galactic latitude. In the figure, the bold solid line shows the distribution of galaxy candidates versus Galactic latitude. The distribution of sample sources which are either known to be galaxies or observed in our low (low *and* high) velocity coverage is shown by the thin solid (dashed) line, whereas the hatched histogram shows the distribution of "nongalaxies" up to our limiting velocity of $\sim$16,000 km s^{-1}. In the region $|b| > 10°$ up to $v_h \sim$ 16,000 km s^{-1}, more than 96% of the 702 sample sources are known to be galaxies or observed in our H I surveys, i.e., the galaxy sample is nearly

TABLE 3

H I 21 CENTIMETER DATA OF THE DETECTED GALAXIES

PSC Source (1)	v_h(50%) (2)	W^m_{20} (3)	W^m_{50} (4)	W^p_{20} (5)	W^p_{50} (6)	W^p_{80} (7)	$\int Svdv$ (8)	S/N (9)	Notes (10)
02076+3111	14166	262	243	259	182	154	1.22	4.9	
02077+2255	14132	117	91	102	62	43	0.43	5.4	
02093+2929	9232	322	309	321	308	271	1.40	4.5	
02146+1605	4040	197	137	144	98	30	0.99	8.6	
02239+1910	4189	323	292	309	280	261	6.35	18.4	
02249+2740	10468	363	346	365	349	336	1.70	5.0	
02256+2156	9043	228	215	228	180	156	0.63	3.8	
02271+2826	4565	333	289	331	285	246	3.75	7.7	
02315+2621	10882	294	288	294	263	245	0.82	4.2	
02433+1544	7677	227	208	228	213	188	0.71	4.1	
02437+1842	9957	409	411	417	385	371	1.92	4.0	
02444+1619	8517	277	235	271	198	146	1.77	6.6	
02451+0522	1519	107	98	104	59	49	0.46	3.1	
02471+1646	11862	352	345	306	269	259	0.97	3.3	
02491+2113	8517	329	275	335	283	259	11.77	30.4	
02493+0902	15215	541	519	498	451	425	2.80	5.0	
02537+0853	10959	275	268	274	265	259	0.42	3.1	
02539+0913	7382	378	353	375	346	326	4.26	7.9	
02569+1022	7420	375	345	355	314	301	1.36	5.0	
02571+1623	9327	297	285	295	273	254	1.12	3.9	
03061+1959	10564	379	340	353	335	310	1.34	5.4	
03079+0018	14224	218	214	217	185	173	0.94	3.1	
03116+2523	9663	274	259	276	240	232	0.64	4.0	
03131+0858	7858	427	408	417	392	368	9.94	20.3	
03188+1322	8497	257	250	255	217	189	0.89	4.3	
03211+1600	11620	439	388	443	389	361	3.95	10.7	
03222+1617	12110	522	508	523	514	444	2.48	6.2	
03238+1748	11599	346	316	340	265	253	1.82	9.1	
03250+1606	7176	92	82	89	74	63	2.64	16.5	
03250+0856	7197	398	390	500	490	466	2.73	4.1	(1)
03275+1535	7917	203	236	279	223	207	2.24	13.0	(2)
03312+0906	5626	307	240	280	246	235	1.92	4.7	
03319+1325	10106	294	261	394	358	346	0.97	3.1	(3)
03347+0619	9930	339	321	332	302	285	2.31	9.3	
03459+1259	6823	402	278	293	270	198	4.41	18.0	
03515+1513	8433	424	414	423	411	347	1.42	4.6	
03550+0609	5388	143	133	140	127	69	1.00	4.5	
03589+3143A	5158	308	277	320	271	247	2.54	10.0	(4)
03589+3143B	5455	93	99	105	58	41	2.54	7.5	(4)
04017+0638	5644	340	300	326	288	262	5.46	7.7	
04082+1351	15831	549	521	583	514	443	2.45	5.8	
04105+2541	6546	350	337	344	327	310	2.80	10.4	
04112+2432	8552	192	169	228	144	128	1.10	5.3	
04139+2737	5298	495	470	494	468	439	3.88	9.3	
04149+0125	4890	249	210	240	197	171	3.75	10.4	
04203+1415	14050	411	404	409	401	392	1.14	4.6	
04210+1303	7792	403	437	533	432	388	3.59	9.2	
04226+0944	5828	262	240	258	217	179	5.05	12.5	
04238+2935	7679	337	327	337	325	268	1.00	4.5	
04250+1037	5460	230	218	224	205	187	4.36	20.0	
04285+0824	4343	232	202	221	188	149	5.66	28.3	
04293+0640	8181	183	139	150	97	67	2.74	20.0	
04303+0932	5465	217	205	211	195	180	2.79	13.5	
04309+1144	4370	331	318	326	310	298	4.42	13.3	
04363+1125	7851	518	491	512	481	457	4.76	10.7	
04372+1225	7931	>292	>298	—	—	—	2.50	8.6	(5)
04380+0024	4516	157	169	203	158	126	1.98	9.4	
04416+2809	3403	353	279	373	240	223	3.47	8.2	
04425+1058	4615	524	510	488	480	473	1.54	3.6	
04513+0104	6889	88	79	84	49	41	0.44	4.1	
05028+2135	5120	282	267	282	263	244	1.17	5.7	
05066+0844	10949	251	254	335	250	174	2.04	8.6	
05100+0614	5932	296	274	294	282	266	2.00	6.3	(6)
05113+0627	8930	305	291	302	286	234	2.49	10.0	
05125+0612	4491	115	99	109	91	73	1.76	13.7	
05187+0450	4266	361	339	347	323	304	9.96	30.0	
05192+0317	4485	222	213	220	209	189	2.00	7.7	
05273+1045	7605	178	172	174	157	147	0.37	4.1	
05316+0246	4016	212	185	208	182	163	3.75	19.0	
05321+3205	2720	90	82	88	77	62	0.31	3.1	
05327+0251	5766	197	182	194	137	69	1.04	4.3	
05339+0825	11140	316	279	297	244	205	1.78	7.3	
05347+0947	5084	262	88	98	68	50	1.23	12.8	
05430+3154	7422	383	351	383	344	314	4.52	12.8	
05537+1331	7731	243	199	236	186	150	1.86	10.0	
06006+2735	5142	313	222	330	264	243	4.40	21.4	
06040+2152	5829	365	345	362	341	322	4.40	14.1	
06339+1921	5312	174	170	218	213	207	0.37	3.4	
06442+3223	5079	155	137	147	126	104	4.91	21.4	
07092+2609	7711	374	330	376	360	322	2.90	6.5	
07238+2821	11589	284	271	278	257	244	0.99	0.5	(7)
07299+0536	14853	119	103	114	92	63	0.49	4.5	
07372+0637	12270	303	296	265	254	247	1.02	4.1	
07595+2734	5228	401	356	380	342	325	5.87	13.0	
08056+1228	10068	366	359	366	333	323	1.38	4.5	
08242+0735	9411	349	333	344	322	304	2.10	7.1	
09014+0139	9174	302	307	290	317	301	0.50	4.4	
09356+0419	6864	464	447	462	441	418	5.37	12.5	
09456+0244	6015	310	299	310	299	289	1.44	5.0	

NOTES.—(1) Widths are ambiguous; (2) The galaxy was detected in the OFF spectrum taken at the same declination as the ON position, but at an R.A. that is 117.0 east of the ON position; (3) The peak widths are probably incorrect; (4) Possibly two galaxies along the line of sight; (5) The high-velocity wing of the profile is slightly beyond our limiting velocity; (6) The galaxy was detected in the OFF spectrum taken at the same declination as the ON position, but at an R.A. that is 91.8 east of the ON position; (7) The galaxy was detected in the OFF spectrum taken at the same declination as the ON position, but at an R.A. that is 109.5 east of the ON position.

complete. For $|b| < 10°$, there are a total of 174 sources in our candidate sample. The observational completeness up to 8000 km s^{-1} is about 80% for $5° < |b| < 10°$.

We estimate the degree of completeness (2) as follows: Our *IRAS* flux criterion implicitly discriminates against H I poor galaxies because the FIR luminosity L_{FIR}, as defined in Lonsdale et al. (1985), correlates with the H I mass, M(H I), for *IRAS* galaxies. Assuming a value of $3.5(L_\odot/M_\odot)$ for the mean ratio of L_{FIR}/M(H I) as in nearby galaxies (i.e., $B^0_T < 12$ and $v_h \lesssim 2000$ km s^{-1}) with $f(60)/f(100)$ colors similar to those considered here (e.g., Young et al. 1989), $f(100)/f(60) = 2.3$, a limiting *IRAS* flux density $f(100) = 1.5$ Jy and a Hubble constant 75 km s^{-1} Mpc^{-1} (a value used throughout this paper), the limiting H I mass M^{limit} as a function of redshift imposed by our IR selection criteria can be computed as

$$\log_{10}(M^{limit}/M_\odot) \approx 7.60 + 2\log_{10}(v_h/10^3 \text{ km s}^{-1}) . \quad (1)$$

TABLE 4

VELOCITY DATA OF THE SG AND NG SUBSAMPLES

Subsample (1)	N_g (2)	$P(v_h)$ (3)	P_1(no v_h) (4)	P_2(no v_h) (5)	$P(v_h < 9k)$ (6)	$P(v_h < 16k)$ (7)
SG	309	88.3%	6.8%	5.2%	63.8%	85.4%
NG.....	318	77.0	5.1	4.1	60.7	70.4

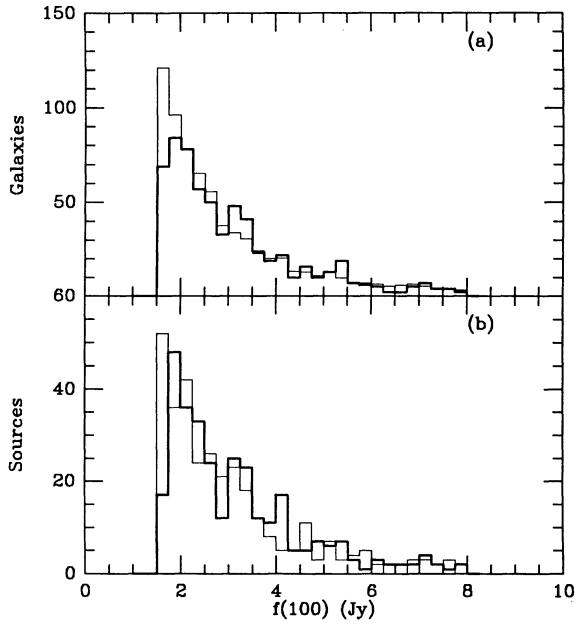

FIG. 2.—(*a*) Comparison of the *IRAS* 100 μm flux density distribution of the combined SG and NG subsamples of 627 galaxies with $|b| > 10°$ (*thick solid line*) with that of a sample of similarly selected 3540 PSC galaxies at $|b| > 35°$ (*thin solid line*). The latter sample has been scaled to show an equal number of galaxies for $f(100) > 3.5$ Jy as the former sample. (*b*) Similar to (*a*), but the comparison is between the SG (*thick solid line*) and NG (*thin solid line*) subsamples. No normalization has been applied.

This function is shown in Figure 4, together with computed H I masses of the detected galaxies. Also shown are the mean H I masses, $\bar{M}$, of spiral galaxies of different morphological types for which we adopted $\bar{M} = 4$, 2, and 1.5 times $10^9\ M_\odot$ for Sab-Sb (*thin solid horizontal line*), Sbc-Sc (*short-dashed horizontal line*) and Scd-Sd (*long-dashed horizontal line*) (see Haynes & Giovanelli 1984; Hoffman et al. 1989). The preselection of equation (1) has to be compared to the sensitivity of the H I survey. Taking the survey sensitivity to be 4.5 mJy (i.e., 3 times

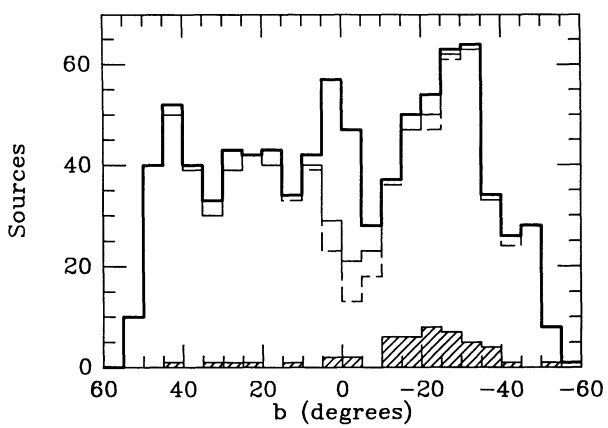

FIG. 3.—Number of sample sources as a function of Galactic latitude *b*. The thick solid line is the distribution of all sample sources, the thin solid (dashed) line indicates the distribution of known galaxies plus those observed in H I up to 8000 (16,000) km s^{-1}. The hatched histogram is the distribution of those sample sources not detected to be galaxies up to 16,000 km s^{-1} in the redshift surveys of this paper and Lu et al. (1990).

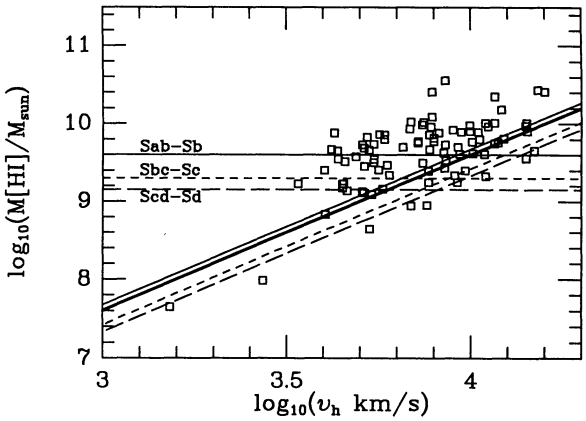

FIG. 4.—Logarithmic H I mass as a function of the logarithmic heliocentric velocity for the galaxies detected in this paper. The H I masses are derived as in Lu et al. (1990) using a Hubble constant of 75 km s^{-1} Mpc^{-1}. The three horizontal lines indicate the mean H I masses of spiral galaxies of morphological types Sab-Sb (*thin solid line*), Sbc-Sc (*short-dashed line*) and Scd-Sd (*long-dashed line*). The approximate limiting H I mass set by the *IRAS* selection criteria is represented by the thick solid line. The three thin lines parallel to it represent the approximate sensitivity of the H I survey for different morphological types, indicated by the same line styles as used for the three horizontal lines.

the observed rms noise), the mean edge-on velocity widths to be 350, 200 and 160 km s^{-1} for the above three morphological bins, respectively, and galaxy disks to be inclined at 45° with respect to the line of sight, we obtained for the sensitivity limit of the H I survey

$$\log_{10}(M^{\rm obs}/M_\odot) \approx M_0 + 2\log_{10}(v_h/10^3\ {\rm km\ s^{-1}}), \quad (2)$$

where $M_0 = 7.82$, 7.57, and 7.48 for morphological bins of Sab-Sb, Sbc-Sc, and Scd-Sd, respectively. This sensitivity limits are also shown in Figure 4 using the same line styles as above to distinguish between the morphological types. A comparison of $M^{\rm limit}$ with $M^{\rm obs}$ in Figure 4 suggests that our survey sensitivity is high enough to detect most late-type galaxies in the candidate list.

The above conclusion assumed a constant extrapolation of the ratio $L_{\rm FIR}/M$(H I) from within a distance of $\sim$2000 km s^{-1} to higher redshifts. This ratio may actually have some dependence on redshift for a flux limited sample because $L_{\rm FIR}/M$(H I) appears to be an increasing function of $L_{\rm FIR}$. However, a comparison between $M^{\rm obs}$ and the corresponding mean H I mass of galaxies in Figure 4 assures that, even if the thick solid line in Figure 4 actually flattens out significantly at high velocities, the potential incompleteness due to the finite survey sensitivity never becomes significant below a velocity of $\sim$9000 km s^{-1}.

We summarize the results of this section as follows: (1) Our galaxy sample suffers from an incompleteness which results in a relative deficiency of candidate sources with $1.5 < f(100) \lesssim 2$ Jy as compared with a similarly-selected sample at high Galactic latitudes. For $|b| > 10°$, the magnitude of this incompleteness is about 10% and the variation of this incompleteness within the sample is on the order of $\sim$4%. (2) Our H I observations are fairly complete up to $v_h \sim 16{,}000$ km s^{-1} for $|b| > 10°$ in the sense that most galaxy candidates have been tested whether they are galaxies, and about 80% complete up to $v_h \sim 8000$ km s^{-1} only for $5° < |b| < 10°$. (3) The sensitivity of our H I survey is such that almost all sample galaxies are detected, at least up to $\sim$9000 km s^{-1} in redshift.

4. SPATIAL DISTRIBUTION OF SAMPLE GALAXIES

4.1. *The Overall Distribution*

In the previous section, we have argued that the degree of nonuniformity in our sample is small, particularly for $|b| > 10°$ and $v_h \lesssim 9000$ km s^{-1}. Therefore, our sample offers a view of galaxy distribution that is largely unbiased by Galactic extinction. In this section, we present a detailed look at the angular and redshift distributions of our galaxy sample.

The sky distribution of all 717 sample galaxies is shown in Figure 5. In order to show the effect of Galactic extinction on optical selections, we have used different symbols for the optically cataloged galaxies (*filled squares*) and the pure *IRAS* galaxies (*open squares*). The percentage of pure *IRAS* galaxies in four equal-area right ascension bins are 33% for the $2^h < \alpha < 4^h$ bin, 53% for the $4^h < \alpha < 6^h$ bin, 43% for the $6^h < \alpha < 8^h$ bin, and 20% for the $8^h < \alpha < 10^h$ bin. The variation of this ratio mainly follows the pattern of the variation of Galactic extinction A_v. A_v is quite small for the last bin of $8^h < \alpha < 10^h$ (Burstein & Heiles 1982), the difference between pure and cataloged *IRAS* galaxies there reflects mostly the selection of galaxies by our criteria. On the other hand, the Galactic plane crosses the two bins between $4^h < \alpha < 8^h$, which explains the high fraction of *IRAS* galaxies there. These numbers suggest that existing optical catalogs of galaxies are at least 33% (=53%–20%) incomplete in the Orion-Taurus region. They also show that the large-scale structure in that region can be examined in a much less biased way with our *IRAS* selected sample.

To characterize the overall velocity distribution of our sample galaxies, we constructed a comparison sample of PSC galaxies at high Galactic latitudes. This sample covers about 43% of the sky. Therefore, the overall redshift distribution of this sample should be much less affected by local structures than our anticenter sample. This sample was constructed in the following manner. First, the 3621 PSC sources at $|b| > 35°$ which pass our flux and color criteria were selected. After excluding 31 sources possibly associated with either the Large or Small Magellanic Clouds and 50 sources possibly associated with Galactic sources, a total of 3540 sources were left and amost all of them are galaxies. Out of these, 3401 (96%) satisfy the QDOT criteria (see Rowan-Robinson et al. 1991). Therefore, for about one out of six randomly selected galaxies in this subsample, redshift data are available from the catalog of Lawrence et al. (1994). We selected those 583 galaxies (1/5.84 of the total of 3401 sources) which are in this redshift catalog. Most of the remaining 139 galaxies (4%) have $f(60)$ flux densities slightly fainter than 0.6 Jy, the limiting flux density used in the QDOT survey, and are uniformly distributed over the sky. For this, we selected a 1-in-6 subsample of 23 galaxies by choosing every 6th sample source in order of right ascension. Redshift data are available for 13 (56%) of them. Combining the above two 1-in-6 subsamples gives our final "high-latitude sample" (hereafter referred to as HL sample) of 606 galaxies. For 590 (97.4%) of them, redshifts are available.

The redshift distribution of the HL sample is shown as a dashed histogram in Figure 6, where the redshifts v_c are with respect to the Local Group ($v_c = v_h + 300 \sin [l] \cos [b]$ km s^{-1} using Galactic coordinates). A flux-limited sample with $f(60) > 0.65$ Jy, which is roughly equivalent to our sample (see § 2), drawn from a homogeneously distributed *IRAS* galaxy population characterized by one of the published 60 μm *IRAS* luminosity functions (e.g., Saunders et al. 1990) would have a distribution which peaks around 4000 km s^{-1}. Compared to such a distribution, there is a deficiency of HL galaxies around this velocity, a phenomenon also observed in other optical or *IRAS* redshift surveys (Geller & Huchra 1989; Strauss & Huchra 1988; Saunders et al. 1990). While some of the difference between the redshift distribution of the HL sample and a simple flux-limited sample is due to the more complicated selection criteria of the HL sample, it might also be affected by a general underdense region between the Local supercluster and its neighboring superclusters. This could lead to a small overestimate of the relative local density $\rho/\langle\rho\rangle$ for small redshifts, if the average density $\langle\rho\rangle$ is taken to be that of the HL sample. Apart from this caveat, the quotient of the histograms for our Galactic anticenter sample and the high-latitude sample can directly be used as an approximation to the relative local density.

In the remainder of this subsection we compare the redshift distribution of the sample galaxies which are located at $|b| > 10°$, i.e., the SG and NG subsamples, with the distribution of the HL sample. We note in Table 4 that for the SG sample the redshift data are effectively complete to 95.1% (i.e., col. [3] + col. [4]) up to about 8000 km s^{-1} and 93.5% (i.e., col. [3] + col. [5]) up to 16,000 km s^{-1}. This means that the resulting velocity distribution is not biased against less obscured regions, where most of previously identified galaxies

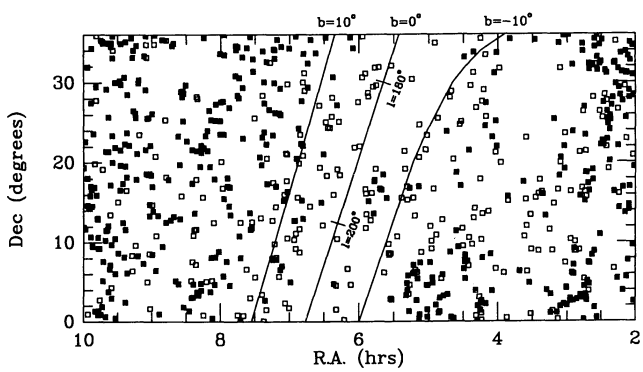

FIG. 5.—Distribution of the 717 sample galaxies in Equatorial Coordinates. Filled squares indicate the (optically) cataloged *IRAS* galaxies and open squares the pure *IRAS* galaxies. Note that the data is less complete for the marked area of $|b| < 10°$.

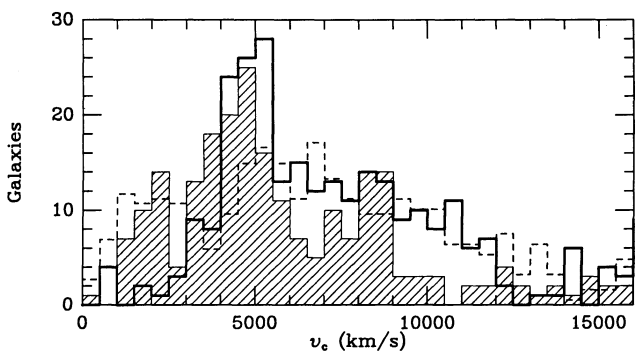

FIG. 6.—Redshift distributions of the SG (*thick solid line*) and NG (*hatched histogram*) subsamples, and of the HL comparison sample (*dashed line*). Only galaxies with available v_c, the velocity with respect to the Local Group, are shown here. The three histograms have essentially equal numbers of galaxies below $v_c = 9000$ km s^{-1}.

(so less likely to be observed in our H I survey) are located. For the NG subsample, the similar completeness percentages in redshift are 82.1% and 81.1%, respectively, due to the fact that many galaxies have unpublished optical redshifts in the "*IRAS*-1.2 Jy" survey (Fisher et al. 1992) and the PSC-Z catalog (Saunders 1994). But in this region, most sample galaxies are optically identified. The resulting (incomplete) redshift distribution should also be largely free from Galactic extinction, but may have a slight bias against large redshifts because optical galaxies with published redshifts may tend to be closer ones. The sample percentages of the HL galaxies with v_h less than 9000 and 16,000 km s^{-1} are 60.9% and 85.1%, respectively. Comparing these numbers with columns (6) and (7) of Table 4 for the NG sample indicates that the redshift data of the NG sample are likely to be fairly complete up to 9000 km s^{-1}, but may suffer up to 15% incompleteness as v_h approaches 16,000 km s^{-1}.

The redshift distributions of the SG and NG subsamples are shown in Figure 6 as the thick solid and hatched histograms, respectively. The dashed histogram of the HL sample has been scaled to have the same number of galaxies below $v_c = 9000$ km s^{-1} as the SG subsample. We note that this normalization should avoid much of the systematic differences between the HL and our anticenter sample. The same histogram scaled to the NG subsample instead would be indistinguishable from the one shown here because both subsamples have almost the same number of galaxies at redshifts less than 9000 km s^{-1} (see Table 4). Excluding those HL galaxies within an 18° radius of the Virgo Cluster would result in a distribution not much different from the dashed one, except for the bin of 500 to 1000 km s^{-1}. Evidently, the distribution of the HL sample shows a significantly smaller fluctuation than that of our SG or NG subsample, especially at $v_c > 4500$ km s^{-1}. This is mainly as a result of its larger angular coverage on the sky although the larger size of the HL sample also results in somewhat better statistics.

The overall density distribution in the part of the survey area with $|b| > 10°$ can be characterized by two "valleys" (or voids) and one major "peak" superposed on an underlying homogeneous distribution. The two voids are at a redshift of less than about 3000 km s^{-1} mainly in the SG subsample and at a redshift of about 7000 km s^{-1} in the NG subsample. These features span more than 1000 km s^{-1} in velocity space and have significances of 5 σ and 3 σ, respectively (assuming Poisson statistics). The peak around $v_c \sim 5000$ km s^{-1} can be seen in both the SG and NG subsamples and has a peak overdensity of ~ 2 and a significance of 5 σ. Galaxy concentrations around this velocity are also observed for $|b| \lesssim 10°$ in our survey area (e.g., Dow et al. 1988; Lu et al. 1990) and in various directions around our survey region (e.g., Focardi, Marano, & Vettolani 1986; Hauschildt 1987; Haynes & Giovanelli 1988; Giovanelli & Haynes 1993, and references therein; Maurogordato et al. 1991; Takata et al. 1994; Seeberger, Huchtmeier, & Weinberger 1994a). As shown below, this peak in the galaxy distribution is due to an excessive number of clusters and superclusters between 4000 and 6000 km s^{-1}. However, these galaxy concentrations do not form a contiguous "wall" in the sense that some of them are not directly connected via a more diffuse wall of galaxies (see §§ 4.2 and 5). Both the SG and NG subsamples also include a small peak around about 8500 km s^{-1}, a velocity close to the peak velocity of the Great Wall (Geller & Huchra 1989). However, this peak is only of a marginal significance of 1.5 σ.

4.2. *Distribution Over Smaller Scales*

The distribution of galaxies over scales much smaller than our survey scale is illustrated by the cone diagrams in Figure 7, where we plot v_c versus the right ascension for the whole survey area (Fig. 7*a*) and for three declination zones of 12 degrees each (Figs. 7*b*–7*d*), up to a redshift of 12,000 km s^{-1}.

To semi-quantitatively characterize structures over scales of order 10 Mpc we have carried out an approximate, model-independent analysis. We chose not to use the HL comparison sample here in order to avoid any bias that could be introduced in a volume normalization. The procedure is as follows: First, we divided the whole survey area into radial shells of 500 km s^{-1} in width. The mean galaxy density in each shell was taken to be the volume average of the number of galaxies with $|b| > 5°$ in that shell. Since we were looking for structures below 9000 km s^{-1} in such an approximate analysis, we could afford to adopt this lower limit in $|b|$ here (see §§ 3.2.1 and 3.2.2 for the degree of sample completeness). The variation of the mean galaxy density as a function of velocity is shown in Figure 8. The superposed dashed curve in the figure is the connection of successive data points with linear segments, where data points judged to be deviant were excluded. It serves as an estimate of the mean density at any given velocity. Subsequently, a three-dimensional cell of a fixed volume was systematically moved around in the survey volume to look for regions where the number of galaxies within the cell is 5 or larger. Once such a region was located, a significance test based on Poisson statistics was performed using the mean galaxy density at the center of the cell. If the test was passed at 3 σ level, the cell was registered as a galaxy concentration. The above scheme was then carried out with an increased cell size for larger structures of low contrast and for merging smaller structures. The cell dimensions were increased with a step size of ~ 500 km s^{-1} in redshift direction and $\sim 5°$ in either angular direction. The maximum dimensions were limited to below ~ 3000 km s^{-1} and $\sim 30°$. Finally, we visually investigated any detected structures for some necessary adjustment (e.g., manually defining the best sizes). Voids were also identified in this way, but without the requirement of a minimum number of galaxies in a cell.

Table 5 lists the final parameters of the detected galaxy concentrations with 10 or more galaxies and the four largest voids with a central velocity less than ~ 9000 km s^{-1}. The column entries from left to right are an assigned ID; the right ascension, declination (1950), the redshift of the center of a structure; the approximate extension in right ascension, declination and redshift; the total number of detected galaxies, N_{obs}; the expected mean number of galaxies, N_{ave}; the significance level taken to be $|N_{obs} - N_{ave}|/(N_{ave})^{1/2}$; and finally identifications and references as explained below.

Several well-known superclusters are detected: S2—the "head" of Pisces-Perseus supercluster (Haynes & Giovanelli 1988), S6—the N1600 supercluster (Saunders et al. 1991), S9—the Gemini filament (Focardi, Marano, & Vettolani 1986); and S11 and S12 are part of the "Great Wall" (Geller & Huchra 1989). S1 appears to be filament-like in Haynes & Giovanelli (1988). S8 appears to be a rich galaxy concentration right behind the Galactic plane even though our data are somewhat incomplete there. This feature was also detected in the optical survey of Takata et al. (1994).

The four voids in Table 5 can be clearly identified in Figure 7*a*. The "nearby void" V0 covers most of our surveyed solid angle and reaches out to a redshift of nearly 3000 km s^{-1}. For

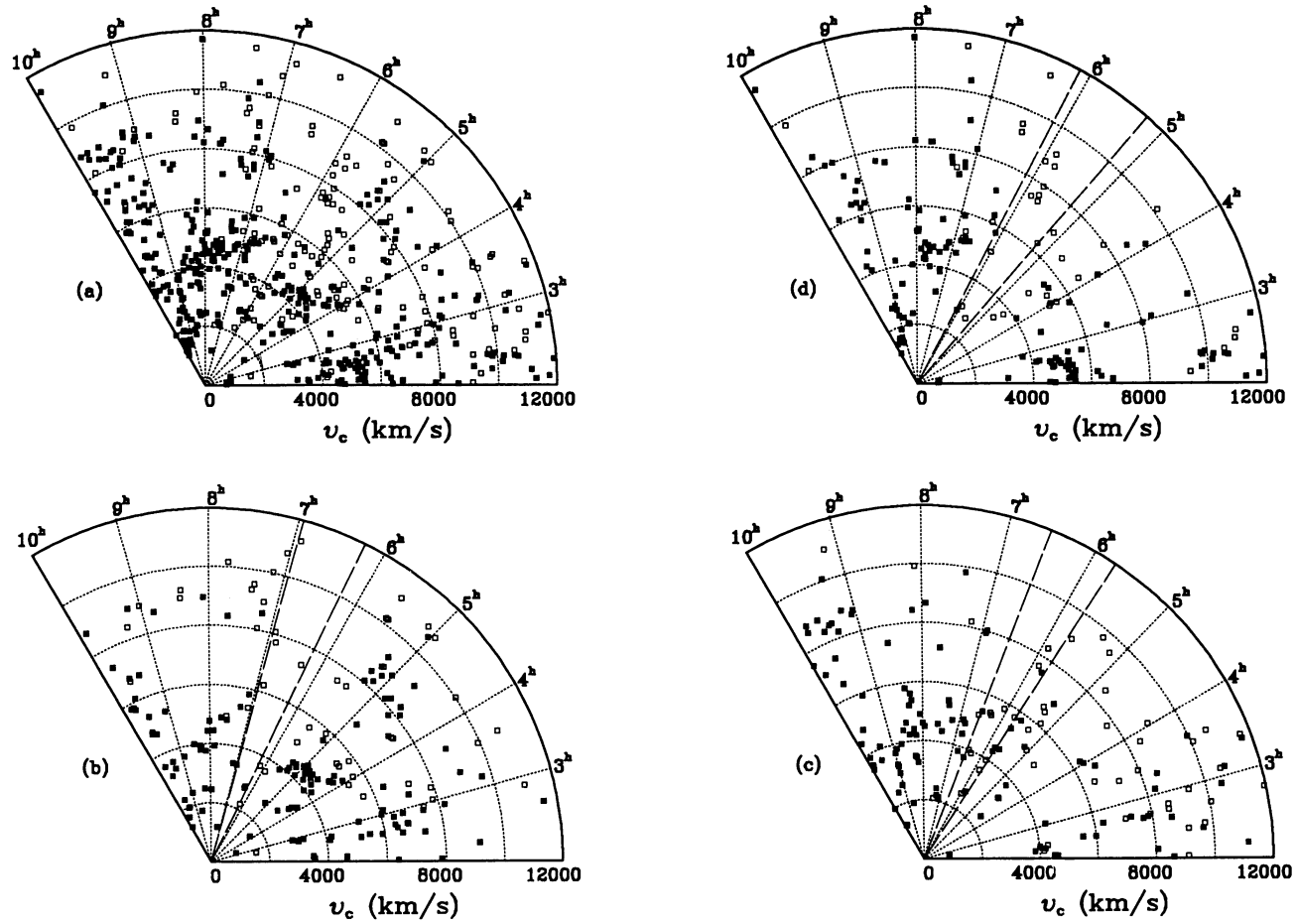

FIG. 7.—Cone diagrams of velocity versus right ascension for various zones of declinations δ: (*a*) the whole survey area, (*b*) $0° < \delta < 12°$, (*c*) $12° < \delta < 24°$, and (*d*) $24° < \delta < 36°$. The symbols are the same as in Fig. 5. The area between the two dashed radial lines in each diagram highlights $|b| < 5°$ where our observations are not quite complete for these diagrams. Note that the solid angles of these diagrams have not been corrected for the cos δ effect. One galaxy with a negative v_c is off scale.

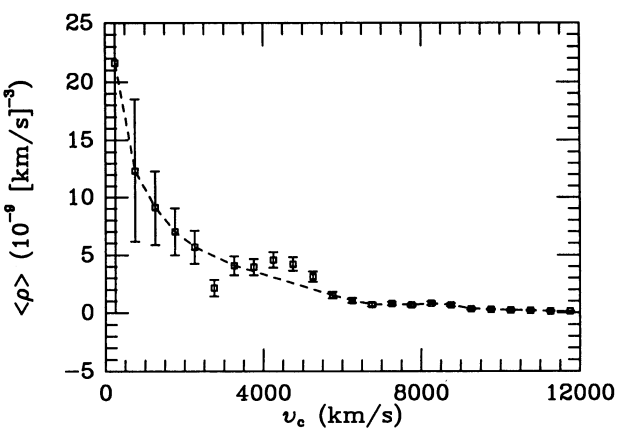

FIG. 8.—Mean galaxy density for the sample galaxies with $|b| > 5°$ as a function of velocity. Each of the squares represents the mean density of a shell of 500 km s^{-1} in width, taken to be the volume average within that shell. The 1 σ error bars shown are computed from Poisson statistics. The dashed curve is made of linear segments which connect successive data points after excluding a few deviant points. The galaxy density is expressed in units of 10^{-9} (km s^{-1})$^{-3}$ or roughly 4×10^{-4} Mpc^{-3} if $H_0 = 75$ km s^{-1} Mpc^{-1}.

this void the formal significance level as given in Table 5 is quite uncertain because of the small number of galaxies and the presence of the void in the calculation of the mean background. However, its high significance has been shown in the comparison with the HL sample as was discussed in § 4.1. The voids V1 and V2 join each other at $\delta \gtrsim 18°$, forming a void which stretches from the Local Group all the way to ~9000 km s^{-1} (or even beyond). A void of this depth could be confused with Galactic extinction in an optical redshift survey, whereas the present survey is by design not vulnerable to such confusion. We note that none of the sample nonuniformities discussed in § 3 are likely to produce a spurious void of such a shape. To further test the reality of these voids we obtained H I spectra over our *low-velocity* coverage for 23 PSC sources (also listed in Table 2) in the general direction of the voids ($3^h < \alpha \lesssim 5^h$), which *failed* passing our selection criteria in one way or another. Two were detected (i.e., 03459+1259 and 04372+1225 with $v_h > 6000$ km s^{-1}), but neither of them is within the boundaries of the voids. For a given solid angle and within our low-velocity coverage, the volume below $v_h \sim 6000$ km s^{-1} (mostly voids in our case) and that above this velocity are roughly equal. One therefore would expect to detect much more than two galaxies in the void regions if galaxies were actually uniformly distributed (because this sample is still flux

TABLE 5

APPROXIMATE PARAMETERS OF LARGE GALAXY CONCENTRATIONS AND VOIDS

ID (1)	α_{1950} (2)	δ_{1950} (3)	v_c (4)	Dimensions (deg × deg × km s^{-1}) (5)	N_{obs} (6)	N_{ave} (7)	$\lvert\delta N\rvert/\sqrt{N_{ave}}$ (8)	References (9)
Large Concentrations								
S1	2.4^h	27^d	9100 km s^{-1}	8 × 8 × 1800	12	1.2	10	Haynes & Giovanelli (1988)
S2	2.5	33	5000	12 × 12 × 1100	25	2.5	14	PP Supercluster
S3	2.7	18	7300	06 × 06 × 3000	11	1.4	8	
S4	3.0	8	6800	15 × 15 × 2000	15	4.0	5	
S5	4.4	9	5500	11 × 11 × 1200	10	3.2	4	
S6	4.9	4	4400	18 × 18 × 1000	22	7.8	5	N1600 Supercluster
S7	5.0	3	8500	15 × 15 × 1500	14	4.9	4	
S8	6.0	20	5900	25 × 05 × 700	10	1.4	7	Takata et al. (1994)
S9	7.8	28	4700	27 × 08 × 700	33	3.3	16	Gemini Filament
S10.....	8.0	6	4300	12 × 12 × 1300	12	4.0	4	
S11.....	9.0	10	9000	38 × 06 × 800	11	2.2	6	Great Wall
S12.....	9.5	16	8500	13 × 13 × 800	10	2.1	5	Great Wall
Large Voids								
V0	5.2	18	1000	97 × 36 × 2000	7	29	4	
V1	3.5	18	3750	15 × 36 × 3500	1	29	5	
V2	3.5	29	8000	25 × 14 × 2000	0	12	3	
V3	8.0	10	7000	30 × 20 × 2000	0	13	4	

limited to $f[100] \approx 1.5$ Jy). Since it is unlikely that the selection of these 23 sources discriminates against PSC galaxies in these void regions, this result confirms that these voids are not affected by the details of our selection criteria. Further supporting evidence comes from that fact that part of these voids are also apparent in denser redshift surveys of optically selected galaxies (e.g., Haynes & Giovanelli 1988; Giovanelli & Haynes 1993). The existence of these voids clearly shows that the Pisces-Perseus supercluster does not extend to $\alpha > 3^h$ within the declination zone of our survey.

The void V3 lies just in front of the Great Wall of the CfA optical redshift survey (Geller & Huchra 1989). As evident in Figure 7, this void appears to extend well into the ZOA. But the striking contrast between the Great Wall and this foreground void appears to be limited only to $b > -10°$ (see also Fig. 6).

5. DISCUSSION

5.1. *On the Extent of the Pisces-Perseus Supercluster*

We have argued in § 3.2.2 that a sample generated by the selection criteria of Table 1 contains only a small percentage of Galactic sources, e.g., less than 15% in the complex Orion-Taurus region are Galactic sources. The construction of the HL galaxy sample indicates that at high Galactic latitudes (i.e., $|b| > 35°$), the contamination of Galactic sources is less than 2%. Lu et al. (1990) have shown that, even at $|b| \sim 3°.5$, a similarly selected sample contains more than 33% galaxies up to $v_h \sim 9000$ km s^{-1} (the limiting velocity there), or more than 46% galaxies up to 16,000 km s^{-1} if an extrapolation is made using the redshift distribution of galaxies in the current sample. Therefore, our selection criteria can be used to extract from the PSC an "all-sky" map which primarily traces the galaxy distribution even in most parts of the ZOA. But there are some related pitfalls: (1) the generated catalog is slightly incomplete at $f(100) \lesssim 2$ Jy at low Galactic latitudes (see § 3), and this incompleteness may become severe within a few degrees of the Galactic plane and toward the Galactic center region. (2) As any galaxy sample drawn from the *IRAS* database, such a map may undersample rich cluster cores which are dominated by gas-poor galaxies, but not structures on scales of superclusters and ridges connecting rich galaxy clusters (e.g., Strauss et al. 1992). (3) Without detailed redshift data, a two-dimensional representation of the data, such as in Figure 9 below, suffers from the projection effect, making a galaxy concentration less eye-catching if there are voidlike regions in front of or behind it (e.g., the Gemini filament in Fig. 9 is less obvious than its appearance in Fig. 7). This effect is somewhat worsened by our stringent color criteria that could filter out up to 50% of *IRAS* galaxies. Nevertheless, a two-dimensional map provides a clear view of the relative geometry of known structures, and with aids of the spectroscopic data from this paper and/or from the literature, we can still draw some fairly confident conclusions.

Figure 9 shows the angular distribution of the selected 7971 PSC sources in Galactic coordinates. An additional 315 sources selected by our criteria are not shown here, of which 31 are associated with either the Large or Small Magellanic Cloud and 284 are identified as Galactic sources in the PSC. The majority of the sources in Figure 9 are galaxies and most of them at high Galactic latitudes or in less obscured regions should have redshifts available soon (Saunders 1994). Here we shall concentrate on the part of the Galactic plane close to the anticenter region in which the galaxy distribution so far has not been discussed in other *IRAS* galaxy samples.

The optically visible part of Pisces-Perseus (PP) supercluster ($140° \lesssim l \lesssim 160°$; $b < -10°$) has been extensively studied (Haynes & Giovanelli 1988; Giovanelli & Haynes 1993, and references therein). These studies of optically selected galaxies have raised the question whether the main ridge of the PP supercluster extends into the ZOA. It is clear from Figure 7 that the PP main ridge does not turn into our survey area. Furthermore, there have been some suggestions that the PP supercluster crosses the ZOA and connects to structures in the northern Galactic hemisphere including the 3C 129 cluster at $l \sim 160°$ and $b \sim 0°$ (Hauschildt 1987) and cluster Abell 569 at $l \sim 170°$ and $b \sim 20°$ (Focardi et al. 1986; Chamaraux et al. 1990). The locations of these two galaxy clusters are marked in Figure 9 by the open and filled squares, respectively. We argue

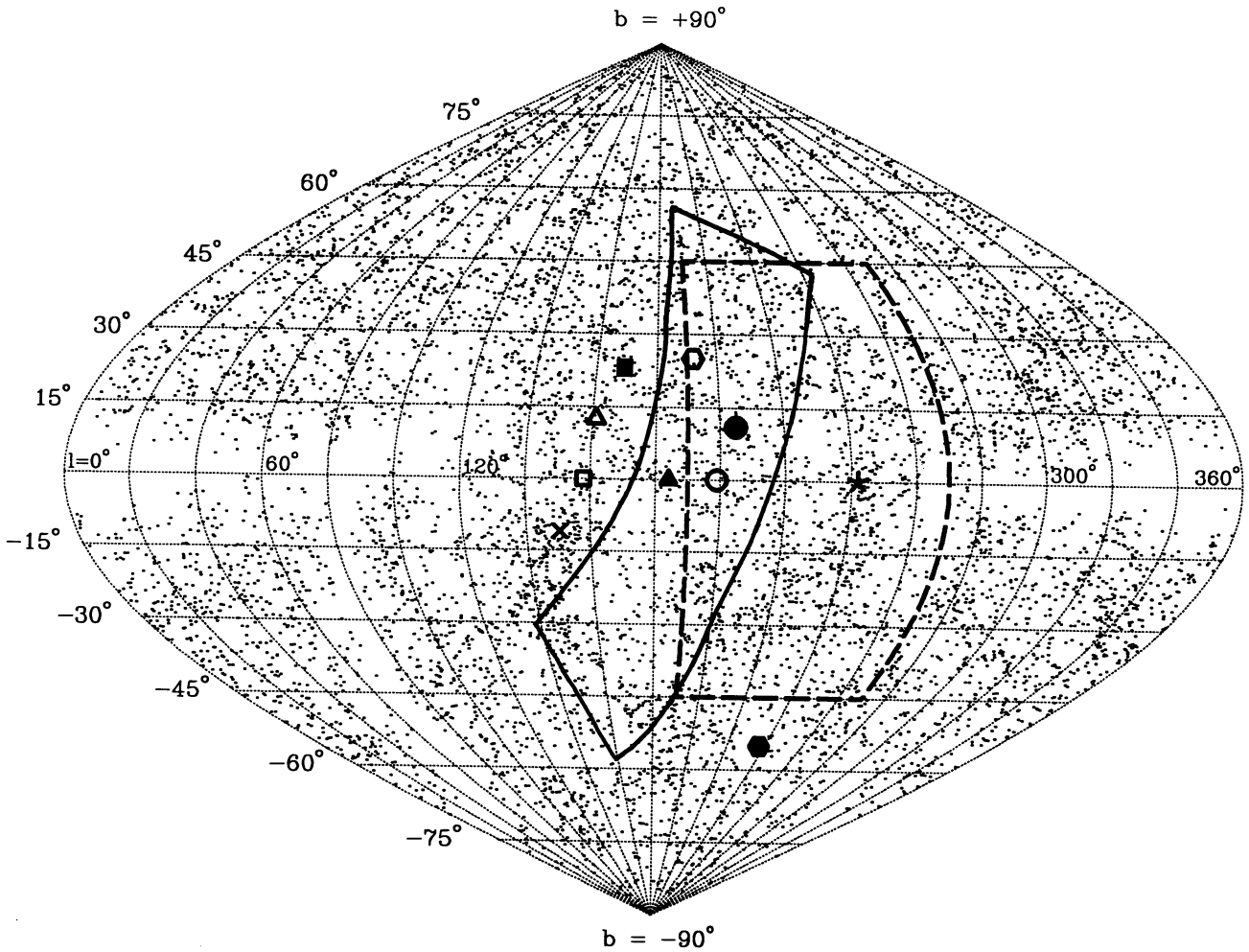

FIG. 9.—Sky distribution of 7971 PSC sources selected using the criteria of Table 1. The thick solid lines enclose the survey region of this paper. The dashed lines enclose the "mirror" image of the Local Void of Tully & Fisher (1987). The locations of several galaxy concentrations are marked in the figure and discussed in the text. These are the main ridge of the PP supercluster (*cross*); the 3C129 cluster (*open square*); a patch of galaxies with $6000 < v < 9000$ km s^{-1} identified by Takata et al. (1994) (*open triangle*); the A569 cluster (*filled square*); galaxy concentration S8 in Table 4 (*filled triangle*); the Gemini filament (*open hexagon*); the Fornax-Eridanus cluster (*filled hexagon*); and the Puppis cluster (*asterisk*). The open and filled circles indicate the directions of the Local Velocity Anomaly given by Faber & Burstein (1988) and by Han & Mould (1990), respectively.

that Abell 569 is unlikely to be connected to the main ridge of the PP supercluster, mainly based on the following facts: (1) The contrast between the source surface density near the position of Abell 569 and that in the PP supercluster is much greater than what is expected from the differential contamination of Galactic sources (~15%). (2) With spectroscopic data, Takata et al. (1994) have shown that most of the galaxies around $l \sim 160°$ and $b \sim 10°$ (marked by the open triangle in Fig. 9) have velocities between 6000 and 9000 km s^{-1} (see their Fig. 6), clearly separating Abell 569 from the main ridge of the PP supercluster. Their spectroscopic data also show that *IRAS* galaxies around 3C 129 have a velocity distribution centered roughly at 5000 km s^{-1}, but with a large dispersion. It is therefore still possible that 3C 129 is connected to the main ridge of the PP supercluster, but a connection to Abell 569 can probably be ruled out.

On the other hand, there are some other galaxy concentrations at velocities around 5000 km s^{-1} near the galaxy concentrations mentioned above: a new galaxy concentration at $l \sim 185°$ and $b \sim 0$ (the filled triangle in Fig. 9 or S8 in Table 4; see also Takata et al. 1994), the Gemini filament at $180° \lesssim l \lesssim 210°$ and $15° \lesssim b \lesssim 30°$ (the open hexagon in Figure 9 or S9 in Table 4; see also Focardi et al. 1986). All this confirms our conclusion that there is an enhanced number of galaxies around 5000 km s^{-1} over a quite large area in the anticenter region in and around our surveyed area.

5.2. *On the Origin of the Local Velocity Anomaly*

It is known that the Local Group (LG) and nearby galaxies within about 700 km s^{-1} show additional bulk flow with respect to the surrounding regions (de Vaucouleurs & Peters 1968; Faber & Burstein 1988). If the origin of this motion is gravitational, it must be caused by the irregular distribution of mass roughly within a redshift of 1000 to 2000 km s^{-1}. This "Local Velocity Anomaly" (LVA) was commonly attributed to the "negative" gravitational acceleration of the Local Void of Tully and Fisher (hereafter LV$_{tf}$; Tully & Fisher 1987; see Faber & Burstein 1987 and Han & Mould 1990) or a combination of the LV$_{tf}$ and Puppis and Fornax-Eridanus clusters (Lahav et al. 1993). The LV$_{tf}$ is centered at $l \sim 50°$ and $b \sim 0°$ with a maximum angular extent of 80 to 90° and a depth up to 3000 km s^{-1} (Tully & Fisher 1987). We outlined its mirror

image in Figure 9 with dashed lines. The approximate center locations of both Puppis (at $\sim$2000 km s^{-1}) and Fornax-Eridanus clusters (at $\sim$1200 km s^{-1}) are marked in Figure 9 by an asterisk (*) and a filled hexagon, respectively. From the present study, we know that there is a substantial void below $\sim$3000 km s^{-1} in our surveyed area (and extended somewhat to the left of our surveyed area in Fig. 9). This nearby void partially cancels out the effect of the LV_{tf} on the LG for $l \lesssim 220°$. The detailed effect of the two opposite voids on the LG velocity vector depends on how galaxies trace the mass, and in particular what fraction of the mass is contained in the nearby clusters. But the net gravitational effect on the LG and its vicinity from the combination of the LV_{tf}, our nearby void, Puppis cluster, and Fornax-Eridanus clusters would be more likely to trigger a local anomaly pointing towards somewhere in the southern Galactic hemisphere, outside and to the right of our survey area in Figure 9. The observed directions of the LVA are well within our survey area (marked by the open and filled circles at, respectively, $l \sim 199°$ and $b \sim 0°$ from Faber & Burstein 1988, and $l \sim 205°$ and $b \sim 11°$ from Han & Mould 1990). The separation between the two circles in Figure 9 is about 12 degrees. If this is taken to be the typical error of these measurements, the Puppis cluster itself lies more than 3 σ away, so would probably the predicted LVA direction. Therefore, after taking into account our nearby void, the existing simple gravitational models are probably not sufficient to fully account for the observed LVA, possibly as a result of our still incomplete knowledge of the mass distribution in the local universe.

6. SUMMARY

The region of $2^h < \alpha < 10^h$ and $0° < \delta < 36°$ on the sky crosses the Galactic anticenter part of the Zone of Avoidance (ZOA) and includes most of the highly obscured Orion-Taurus complex region that has been left out of previous galaxy surveys. We have selected a sample of 876 galaxy candidates in this region from the *IRAS* Point Source Catalog and have attempted to detect the 21 cm H I line of those sample sources which were not known to be galaxies in order to identify the galaxies among them. We detected 89 galaxies from the observations of 272 candidates up to $\sim$16,000 km s^{-1} in velocity. Combining our survey with existing data results in a sample of 717 galaxies which is more than 90% complete and within 4% uniform in the region 10° above the Galactic plane and for velocities up to at least 9000 km s^{-1}.

The galaxy distribution in the survey area was analyzed by numeric comparisons of the angular and redshift distributions of this galaxy sample with a control sample at high Galactic latitudes and with the smoothed radial distribution of the sample galaxies, from which we arrived at the following conclusions: (1) We have identified several large voids. In particular, a large void between $\alpha \approx 3^h$ and 4^h, up to $v_h \sim 6000$ km s^{-1}, separates the Pisces-Perseus (PP) supercluster at $\alpha < 3^h$ from structures at $\alpha > 4^h$. This clearly shows that the PP main ridge does not turn into our survey area. (2) Our data extended several optically known galaxy concentrations and revealed some new ones. The existence of a "nearby void" below 3000 km s^{-1} and a lack of any evidence for a nearby galaxy concentration or a moderate overdensity from the outskirts of a nearby rich cluster, rules out the possibility of a major gravitational source in our survey area for the "Local Velocity Anomaly." (3) There is an overall excess of galaxies around $v \sim 5000$ km s^{-1} in the survey area, consistent with the general pattern of the galaxy distribution in and around our survey area. (4) The contrast between the "Great Wall" at $v_h \sim 8500$ km s^{-1} and its foreground void appears to gradually diffuse out after it enters the ZOA from the northern Galactic hemisphere.

Based on our galaxy sample and other redshift surveys around the anticenter part of the ZOA, we have also shown that (1) the main ridge of the PP supercluster does not likely extend to Abell 569, a cluster in the northern Galactic hemisphere; and (2) that the simple gravitational models consisting of the Local Void of Tully & Fisher (1987), our nearby void, and Puppis and Fornax-Eridanus clusters would predict a local velocity anomaly whose direction is probably too far away from that derived from observations.

We wish to thank the staffs of Arecibo Observatory, especially, D. Altschuler, W. Baan, and J. Harmon for their kind help and assistance during the course of our observations. We are grateful to W. Baan for providing us with the calibration data; to J. Eder and L. Hoffman for observing some of our sources; to C. Pantoja, W. Saunders, M. Strauss, and T. Takata for sending us their unpublished or machine-readable data; and to an anonymous referee for carefully reading the manuscript and for various comments and suggestions that improved this paper appreciably. Part of the observations were made remotely. The help from telescope operators was highly appreciated. This work has made use of NASA/IPAC Extragalactic Database which is operated by the Jet Propulsion Laboratory, California Institute of Technology, under contract with the National Aeronautics and Space Administration (NASA); and was in part carried out at the Jet Propulsion Laboratory under a contract with the NASA.

REFERENCES

Böhm-Vitense, E. 1956, PASP, 68, 430
Burstein, D., & Heiles, C. 1982, AJ, 87, 1165
Chamaraux, P., Cayatte, V., Balkowski, C., & Fontanelli, P. 1990, A&A, 229, 340
de Vaucouleurs, G., & Peters, W. L. 1968, Nature, 220, 868
de Vaucouleurs, G., de Vaucouleurs, A., Corwin, H. G., Buta, R. J., Fouqué, P., & Paturel, G. 1993, The Third Reference Catalogue of Bright Galaxies (Springer: New York)
Dodd, R. J., & Brand, P. W. J. L. 1976, A&AS, 25, 519
Dow, M. W., Lu, N. Y., Houck, J. R., Salpeter, E. E., & Lewis, B. M. 1988, ApJ, 324, L51
Fitzgerald, M. P. 1974, A&A, 31, 467
Faber, S. M., & Burstein, D. 1988, in Large-Scale Motions in the Universe, ed. V. C. Rubin & G. Coyne (Princeton: Princeton Univ. Press), 115
Fisher, K. B., Strauss, M. A., Davis, M., Yahil, A., & Huchra, J. P. 1992, ApJ, 389, 188
Focardi, P., Marano, B., & Vettolani, G. 1986, A&A, 161, 217
Geller, M. J., & Huchra, J. P. 1989, Science, 236, 897
Giovanelli, R., & Haynes, M. 1993, AJ, 105, 1271
Han, M., & Mould, J. 1990, ApJ, 360, 448
Hauschildt, M. 1987, A&A, 184, 43
Haynes, M. P., & Giovanelli, R. 1984, AJ, 89, 758
———. 1988, in Large Scale Motions in the Universe, ed. V. C. Rubin & G. Coyne (Princeton: Princeton Univ. Press), 31
Helou, G., Madore, B. F., Schmitz, M., Bicay, M. D., Wu, X., & Bennett, J. 1991, in Databases and On-Line Data in Astronomy, ed. M. A. Albrecht & D. Egret (Dordrecht: Kluwer), 89
Henning, P. A. 1994, in ASP Conf. Ser. 67, Unveiling Large-Scale Structures behind The Milky Way, ed. C. Balkowski & R. C. Kraan-Korteweg (San Francisco: ASP), 203
Hoffman, G. L., Helou, G., Salpeter, E. E., & Lewis, B. M. 1989, ApJ, 339, 812
IRAS Point Source Catalog, Version 2. 1988, Joint *IRAS* Science Working Group (Washington: GPO) (PSC)
IRAS Catalogs and Atlases: Explanatory Supplement. 1988, ed. C. A. Beichman, G. Neugebauer, H. J. Habing, P. E. Clegg, & T. J. Chester (Washington: GPO) (PSC)

Kerr, F. J., & Henning, P. A. 1987, ApJ, 320, L99
Kraan-Korteweg, R. C. 1991, in ASP Conf. Ser. 15, Large-Scale Structures and Peculiar Motions in the Universe, ed. D. W. Latham & L. N. da Costa (San Francisco: ASP), 165
Kraan-Korteweg, R. C., Loan, A. J., Burton, W. B., Lahav, O., Ferguson, H. C., Henning, P. A., & Lynden-Bell, D. 1994, Nature, 372, 77
Kraan-Korteweg, R. C., & Woudt, P. A. 1994, in ASP Conf. Ser. 67, Unveiling Large-Scale Structures behind The Milky Way, ed. C. Balkowski & R. C. Kraan-Korteweg (San Francisco: ASP), 89
Lahav, O., Yamada, T., Scharf, C., & Kraan-Korteweg, R. C. 1993, MNRAS, 262, 711
Lawrence, A., et al. 1994, preprint
Lonsdale, C. J., Helou, G., Good, J. C., & Rice, W. 1985, Cataloged Galaxies and Quasars Observed in the *IRAS* Survey (Pasadena: JPL)
Lu, N. Y., Dow, M. W., Houck, J. R., Salpeter, E. E., & Lewis, B. M. 1990, ApJ, 357, 388
Maurogordato, S., Proust, D., & Balkowski, C. 1991, A&A, 246, 39
Meurs, E. 1994, in ASP Conf. Ser. 67, Unveiling Large-Scale Structures behind The Milky Way, ed. C. Balkowski & R. C. Kraan-Korteweg (San Francisco: ASP), 249
Nilson, P. 1973, Uppsala General Catalogue of Galaxies (Uppsala: Uppsala Astron. Obs.) (UGC)
Pantoja, C. A., Giovanardi, C., Altschuler, D. R., & Giovanelli, R. 1994, AJ, 108, 921
Rowan-Robinson, M., Saunders, W., Lawrence, A., & Leech, K. 1991, MNRAS, 253, 485
Saunders, W. 1994, private communication
Saunders, W., Rowan-Robinson, M., Lawrence, A., Efstathiou, G., Kaiser, N., Ellis, R. S., & Frenk, C. S. 1990, MNRAS, 242, 318
Saunders, W., et al. 1991, Nature 349, 32
Saitō, M., Ohtani, H., Asonuma, A., Kashikawa, N., Maki, T., Nishida, S., & Watanabe, T. 1990, PASJ, 42, 603
Saitō, M., Ohtani, H., Baba, A., Hotta, N., Kameno, S., Kurosu, S., Nakata, K., & Takata, T. 1991, PASJ, 43, 449
Seeberger, R., Huchtmeier, W. K., & Weinberger, R. 1994a, A&A, 286, 17
Seeberger, R., Saurer, W., Weinberger, R., & Lercher, G. 1994b, in ASP Conf. Ser. 67, Unveiling Large-Scale Structures behind The Milky Way, ed. C. Balkowski & R. C. Kraan-Korteweg (San Francisco: ASP), 81
Strauss, M. A. 1994, private communication
Strauss, M. A., Davis, M., Yahil, A., & Huchra, J. P. 1990, ApJ, 361, 49
Strauss, M. A., & Huchra, J. 1988, AJ, 95, 1602
Strauss, M. A., Huchra, J. P., Davis, M., Yahil, A., Fisher, K. B., & Tonry, J. 1992, ApJS, 83, 29
Takata, T., Yamada, T., Saitō, M., Chamaraux, P., & Kazés, I. 1994, A&AS, 104, 529
Tully, B. R., & Fisher, R. 1987, Nearby Galaxies Atlas (New York: Cambridge Univ. Press)
Vorontsov-Velyaminov, B. A., & Arhipova, V. P. 1964, Morphological Catalog of Galaxies (Moscow: State Univ.)
Wakamatsu, K.-I. 1994, in ASP Conf. Ser. 67, Unveiling Large-Scale Structures behind The Milky Way, ed. C. Balkowski & R. C. Kraan-Korteweg (San Francisco: ASP), 131
Weinberger, R. 1980, A&AS, 40, 123
Yamada, T., Takata, T., Djamaluddin, T., Tomita, A., Aoki, K., Taketa, A., & Saitō, M. 1993, ApJS, 89, 57
Young, J. S., Xie, S., Kenney, F. D. P., & Rice, W. 1989, ApJS, 70, 699
Zwicky, F., Herzog, E., Karpowicz, M., Kowal, C. T., & Wild, P. 1961–1969, Catalog of Galaxies and Clusters of Galaxies (Pasadena: California Inst. Tech.) (CGCG)